LATENT HEAT FLUX AND SOUTH AFRICAN SUMMER RAINFALL VARIABILITY

Shaun Courtney

Thesis submitted to the University of Cape Town in fulfillment of the requirements of the degree of Master of Science

November 10, 1997

Abstract

The main purpose of this study was to determine if a relationship exists between oceanic latent heat flux and the summer rainfall of South Africa. Such a link would be useful for a better understanding and the prediction of monthly variability in the summer rainfall for South Africa.

In order to investigate possible relationships between oceanic latent heat flux and summer rainfall in South Africa, point to point and point to field statistical correlations were made between gridded monthly COADS derived bulk oceanic heat fluxes and area averaged rainfall for the period 1950 to 1988.

Correlations with the oceanic latent heat flux were not significant when the summer area averaged rainfall was divided into early and late summer seasons. This is due to the fact that different oceanic latent heat flux regions correlate with a different rainfall region each month.

The results of monthly latent heat flux and summer rainfall demonstrated that there exists a statistical link between oceanic latent heat flux and summer rainfall and that this link could prove useful in the prediction of summer rainfall patterns. These results of the correlation between monthly latent heat flux and summer rainfall show that summer rainfall can be grouped into an all–area index that can be used as a proxy for the entire summer rainfall region. Results of these correlations further show that there are three major mechanisms that are at work over the six month summer rainfall period. These mechanisms show a link between the oceanic latent heat flux and summer rainfall variability.

This study has shown that various oceanographic areas in the surrounding oceans correlate at different lags with South African summer rainfall. These correlations can be useful as precursors in predicting wetter or dryer rainfall events. Areas identified by correlation of oceanic latent heat flux regions as important as precursors for summer rainfall prediction are similar to those areas other researches have identified in studies using OLR, SST and upper level winds (Jury 1995). This study adds weight to the already existing knowledge of these precursors of rainfall predictability.

Acknowledgments

I would like to thank the following:

- My supervisor, Frank Shillington and others in the Department of Oceanography at the University of Cape Town who were willing to help when needed and had the patience to wait for the final result.
- My wife, Jenni, for tireless re–reading of this dissertation and a belief that at last, one day it will be finished. Thank you.

Contents

List of Figures

List of Tables

Chapter 1

Introduction

1.1 Context

Internationally the study of climate and its variability has received a high priority. The International Council of Scientific Unions and the World Meteorological Organisation have recognised the need to understand and predict climate change and its variability (Tyson 1986) . Climate changes over the inter-annual time scale affect countless millions of people around the globe. This is especially true in regions where the population relies heavily on agriculture and stock farming for basic foodstuffs, such as in southern Africa. Relatively small changes in the climate, especially rainfall can have devastating effects

It would therefore be useful to predict these kinds of natural fluctuations in rainfall so that one could be able to manage the associated problems more effectively. Estimates of the transfer of latent, sensible and moisture fluxes between the ocean and atmosphere may provide crucial insight into the dynamics of interannual and decadal climate fluctuations (Esbensen and Reynolds 1981). Studies suggest that a 5 to 10 % change in the net global heat flux over the oceans would have a significant impact on climate analyses (Foster and Brown 1994). Studies of the general circulation and of climate processes in particular must fail if the atmosphere-ocean interaction is not well understood (Ruprecht and Simmer 1991).

Using the Budyko-Lettau dryness ratio it has been shown that most of southern Africa is dry. This ratio is of

mean annual net radiation to the product of mean annual rainfall and latent heat of evaporation. For more than half of southern Africa, the average annual net radiation can evaporate the local average rainfall by a factor of two. In the western interior this factor rises to over ten (Tyson 1986).

Given these conditions the effective management of water resources is critical. This task can be facilitated if reliable long-term predictions of local rainfall can be made. The interannual prediction of rainfall has been tackled by looking at the relationships of rainfall to the Southern Oscillation, the El Niño, Sea Surface Temperature (SST) and Outgoing Longwave Radiation a(OLR). In this dissertation we look at the influence of oceanic latent heat flux on monthly rainfall variability in the summer rainfall region of South Africa.

Current knowledge of the variation of South African rainfall patterns.

Tyson (1984) showed that there is a variance in the annual rainfall over South Africa that can be accounted for by quasi-periodicities of the order of 18 to 21 years. A conceptual model of the wet-spell and dry-spell situations was developed and is shown in figure 1.1. In the wet-spells the ascending limb of the Walker Cell is situated over tropical Africa. The upper tropospheric zonal flow at 20 ° S becomes anomalously easterly and the lower atmosphere becomes westerly. At 30 ° S the zonal anomaly is westerly at upper levels and easterly at 500mb and below. The Zonal flow in the subtropical jet to the south of the continent is strengthened, less in the region of Gough Island and more in the vicinity of Marion Island. During the dry spells the pattern of zonal wind anomalies is the opposite in all respects (Tyson 1986).

A model of the anomalous meridional circulations over southern Africa was also developed. This is shown in figure 1.2

On the synoptic scale, Harrison (1984) developed a synoptic classification system, in which he identified summer systems. These include cloud bands connecting the tropical and temperate circulations, tropical and subtropical cyclones, coastal depressions, cyclones on the continental west coast and the troughs associated with cold fronts on the eastern coast. According to this classification is has been found that the cloud bands connecting the tropical circulations and the mid-latitude cyclones are the major contributors to rainfall over the interior of the country. Harrison (1984) suggests that further research into the causes of summer rainfall variability over South Africa should focus primarily on the formation of these bands.

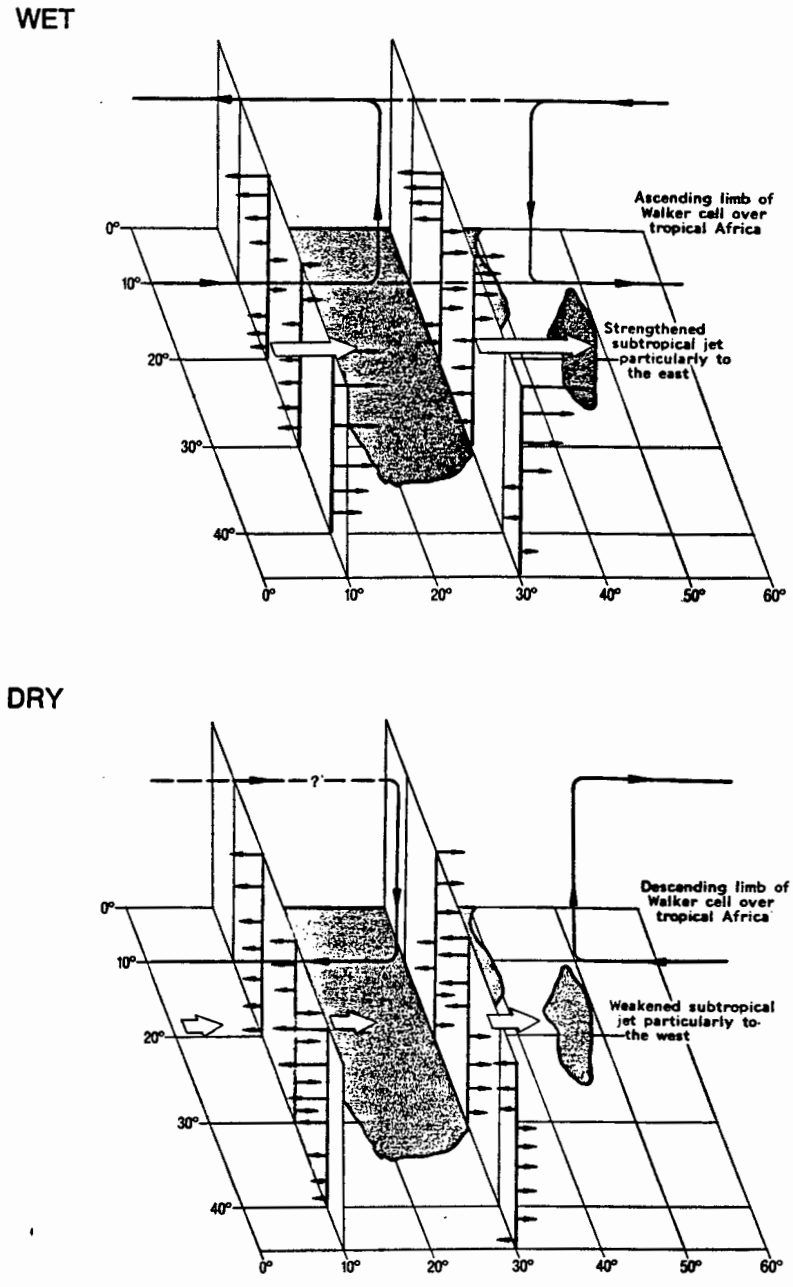

Figure 1.1: A model of zonal wind component anomalies over southern Africa during spells of years predominantly wet and dry conditions (Tyson, 1984)

Lindesay (1988b) examined the spatial and temporal effects of the Southern Oscillation in its extreme phases on rainfall over central South Africa. She found that during the late summer season the Southern Oscillation Index is positively correlated with rainfall over much of South Africa. At most about 20 % of the rainfall variance is explained

by this relationship. The relationship is such that high rainfall tends to coincide with the high phase of the Southern Oscillation and vice versa.

Walker (1989) undertook a study to determine the links between the sea surface temperature and rainfall relationships. She found that the relationship was strongest when extreme global-scale atmospheric events, such as the Southern Oscillation, were excluded from the time series. The presence of positive SST anomalies east and south of Africa increase the likelihood of the formation of Tropical-temperate troughs by intensifying tropical and temperate components. Using this relationship results indicated that SST is a useful indicator of late summer rainfall. This work has provided a starting word and a basis for further research to investigate possible dynamical links between SST and rainfall.

More recently Pathack, Jury, Shillington, and Courtney (1993) undertook a study to provide a statistical basis for the prediction of South African rainfall anomalies on the monthly to seasonal time scales using SST and OLR. It is well known that the SST is an important factor in influencing the generation and sustenance of large-scale deep convection. The relationship between SST and convection is not uniform and shows spatial and temporal variations. To confirm and complement the observed relationship, tropical circulation patterns were also examined. Statistical relationships are shown to hold for December to March. Results of the investigations suggest that vertical tropospheric systems are among the important components which modulate South African Climate. Pathack, Jury, Shillington, and Courtney (1993) , however, suggest that further work needs to be undertaken using more and better data sets. Testing observed results through the use of General Circulation Models (GCMs) was also encouraged.

Scope of this dissertation

Based on the knowledge that SST and summer rainfall is correlated, this study focuses on the relationship of oceanic latent heat flux and the summer seasonal monthly rainfall patterns of South Africa. Using the COADS data set and rainfall data from the Computer Center for Water Research oceanic latent heat flux anomalies in nine "key–box" regions and rainfall anomalies in eight zones were correlated, using both Pearson and Spearman Rank correlation coefficients over a period of 37 years. The oceanic latent heat flux was calculated from monthly variables using the Bulk Aerodynamic Method formula. This method was chosen, although it suffers from some known problems, because we needed to be able to calculate historical oceanic heat flux over large areas, often with sparse data coverage.

Objectives of this study

The main objective of this study was to determine if there is a useful link between oceanic latent heat flux and South Africa's summer monthly rainfall patterns. Useful in the sense that it adds to our knowledge and it is useful in the sense that with this we can effectively predict to some degree the rainfall variability.

Approach and Overview

In Chapter Two we review the work that has been done in historical calculations of oceanic heat flux starting with the work of Bunker (1976) and reviewing the progress that has been made in the calculation of oceanic heat flux over large areas of the ocean. There the focus is on how these oceanic heat fluxes were calculated. This study uses the Bulk Aerodynamic Formulae and so the problems associated with using this method, the different forms of the transfer coefficients and methods of calculation are examined. Lastly we consider the effect that these oceanic heat fluxes have on weather and climate to show that there is some measurable and useful effect of oceanic heat flux and especially latent heat flux on weather and climate.

In Chapter Three the field of study is narrowed to examine previous studies undertaken to determine what is the patterns of rainfall distribution and what effects these mechanisms have on South Africa rainfall. Here a classification of the rain bearing systems is presented and we discuss the relationships of the Southern Oscillation Index and SST on rainfall.

In Chapter Four the rainfall data and the selection of the eight areas are presented. Next the COADS data set, that has been used in this dissertation, is introduced and the methods of calculating the derived variables from the data are shown. This derived data is the data that has been used in this study. The rainfall is grouped into eight rainfall zones. The data is then standardised using the formulas give in the appendix. Once the latent and sensible heat flux has been calculated from the derived variables it was also standardised.

In Chapter Five the results that were obtained from a point-to-field correlation study and the correlation of the key–box areas with rainfall in each the eight zones are reported. The latent heat flux anomalies are correlated firstly in a point-to-field correlation with each of the rainfall zones. These results tended to be poor showing lack of coherence in both the spatial and temporal scales. Following on from the work of Pathack, Jury, Shillington, and Courtney

(1993) the correlation of latent heat flux anomalies in seven key–boxes are considered. These results are tabulated and attention is drawn to the relevant boxes and there correlation with the rainfall in each of the zones.

In Chapter Six the results of the study are discussed and interpretated. Here the temporal and spatial patterns that exist in the results are discussed. The conclusions and future work are included in this chapter.

The Appendix lists the statistical methods and tests that were used in this study.

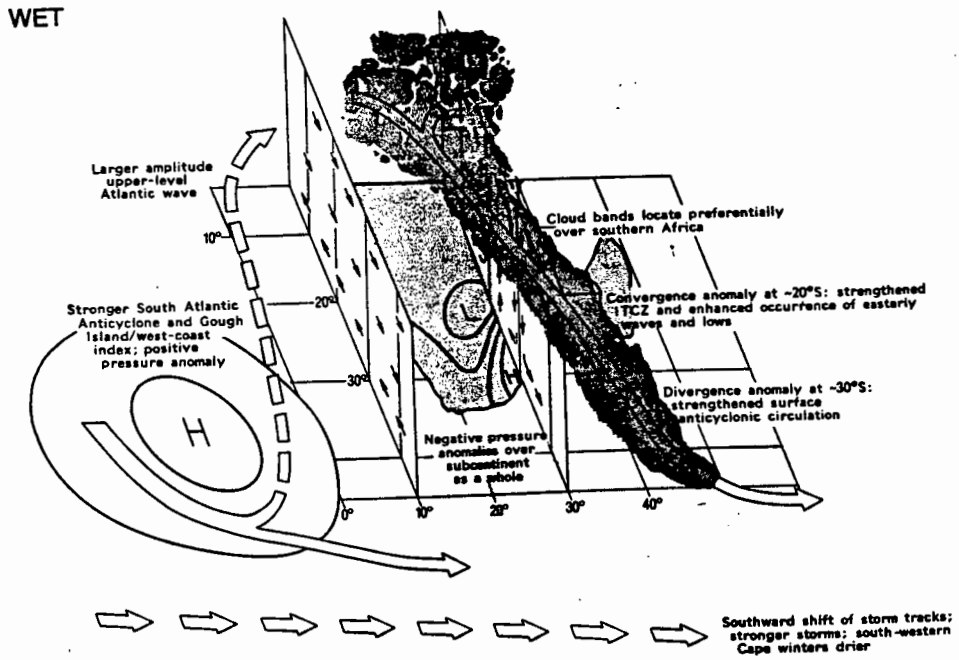

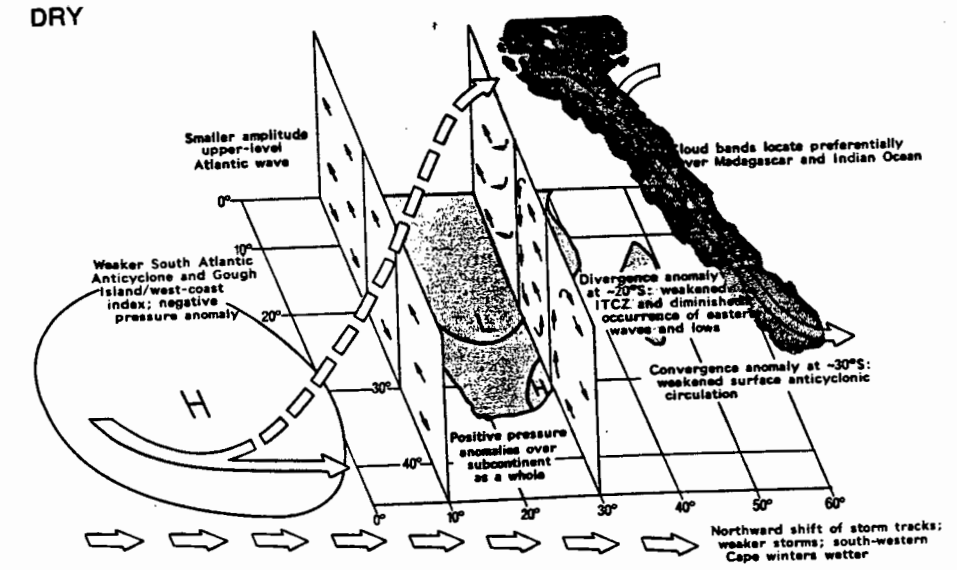

Figure 1.2: A model of the anomalous meridional circulations over southern Africa during spells of years of predominately wet or dry conditions. The relative positions of the upper tropospheric Atlantic wave, preferred zones for cloud-band formation, the surface manifestations of the South Atlantic Anticyclone and location of storm tracks are also shown. (Tyson, 1984)

Chapter 2

Literature Review

We begin this chapter by introducing the necessary background in the form a review of the relevant literature. Firstly, we look at the historical calculation of heat flux from the time of Bunker in the late 1970's to the early 1990's. Secondly, we focus more specifically on the use of the Bulk Aerodynamic Formulae and the problems encountered in calculating heat flux with this method. Thirdly, we look at the effect that these fluxes have on climate.

2.1 Historical calculations of heat flux

An understanding of the global transport of moisture, heat and momentum energy is necessary for the understanding of natural fluctuations in weather patterns over a localised region. The calculations of heat flux are necessary to determine the influence of the oceans on the atmosphere (Esbensen and Reynolds 1981) .

The work of Bunker (1976) has been considered as a base study for historical heat flux calculations in this dissertation. Before Bunker (1976), meteorologists and oceanographers attempted, for many decades, to calculate the total flux of energy across the ocean surface. The main problem encountered with the calculation of these fluxes was that they required parameters measured with sophisticated instruments. From a logistical perspective it is clear that it would not be possible to use this method on a global scale. It is here that the bulk aerodynamic method comes into its own. The Bulk Aerodynamic Method is an easy method that can be used to calculate the flux in areas that have

complete weather and sea surface temperature (SST) observations, as these climatic variables can be used as a proxy and using them the relevant fluxes can calculated.

Bunker (1976) used the National Climate Center data which has approximately 20 million observations. He stated that if the bulk formulas could be improved, reasonably accurate fluxes could be obtained in nearly all areas of the oceans. To do this he used parameterisation to find the appropriate transfer coefficients that were derived from the published results of many previous experiments. Using the bulk formulas and tables he calculated the latent, sensible and momentum fluxes for the North Atlantic Ocean using the above data. His methodology differed from previous studies as he computed the fluxes for each simultaneous measurement of surface meteorological values. The results were averaged to find monthly and yearly values.

These results compared favourably to previous studies especially those by Budyko (1963) , who according to Esbensen and Reynolds (1981), used the bulk aerodynamic method with constant transfer coefficients. These studies showed that the bulk aerodynamic method on monthly averaged data could be used on a basin scale to calculate sensible, latent and momentum fluxes.

Hsiung (1986) surveyed the global oceanic variability through the analysis of seasonal variations of the components of energy balances (incoming and outgoing radiation, sensible and latent heat fluxes) at the ocean surface, using the Tape Data Format (TDF, see section 4.2.1) data set. Unlike the research carried out before, with the exception of Budyko, Hsiung did not limit the calculations to a particular region. Budyko published a world atlas of heat budget, but according to Hsiung (1986) the data sources that he used were not clear. (Another global map by Esbensen and Kushnir, 1981, was calculated from climatological means rather than monthly observations.)

Using the TDF 11 data, averaged into a total of 372 monthly 5° squares for the years 1948–1979 Hsiung calculated the balance of energy flux (Q_{net}). This consisted of calculating the latent (Q_l) and sensible flux (Q_h), and the incoming (Q_{in}) and outgoing radiation (Q_{out}):

$$Q_{net} = Q_{in} - Q_{out} - Q_h - Q_l \tag{2.1}$$

The values Bunker used for the latent heat transfer coefficient (C_E) were specified as a function of stability and wind speed from the results of previous studies. To calculate saturated specific humidity (q_s) and specific humidity

(q), the following equation was used:

$$q = \frac{0.622 e_s}{p - 0.378 e_s} \tag{2.2}$$

where:

e_s is the saturation vapour pressure and

p is the pressure at sea level

To calculate the value q, e_s is calculated using dew point temperature and to calculate the value q_s, e_s is calculated using sea surface temperature (SST). e_s itself is computed using a polynomial approximation as a function of temperature (see equation 4.1).

The results Hsiung (1986) obtained were then used to calculate monthly and annual means. The monthly means were calculated for one month in each season, more specifically January, April, July and October. It was found that there is a large seasonal variation in the distribution of latent heat flux. However, in contrast with latent heat flux, sensible heat flux had little spatial variation. The only exception was in January when warm western boundary currents in both the Pacific and Atlantic oceans set up large temperature gradients between the relatively cold atmosphere and warm ocean. The associated winds, in January are stronger and produced a larger sensible heat flux loss in the Northern Hemisphere. When examining the annual means it was quite clear that of the two heat fluxes, latent heat is overwhelmingly dominant over sensible heat flux. Hsiung stated that the net radiation is mostly a balance between incoming radiation and latent heat flux.

Gueremy (1990) studied the low frequency variability of sensible and latent heat flux over the Indian monsoon region. The three main findings are summarised as follows: firstly, the variability of specific humidity was found to be greater over the land than over the oceans on the intra-seasonal scale; secondly, the wind provides a major influence on the surface fluxes, especially over the latent heat over the oceans; and thirdly a close relationship between the propagation of low frequency waves and the propagation of surface heat flux was found. This, according to Gueremy, suggested a feedback mechanism which related surface processes to the northward propagation of these waves over Indian Monsoon Area. Gueremy used the following data for his calculations: The First GARP Global Experiment analysed data, the TIROS-N outgoing radiation data and the Monsoon Experiment precipitation data.

Crewell, Ruprecht, and Simmer (1991) used *Nimbus-7* Scanning Multi-frequency Microwave Radiometer (SMMR)

data and ship observations to compute the latent heat flux via the bulk aerodynamic method over the North Atlantic Ocean. The SST and surface humidity were determined from microwave data. The surface wind speed was derived from an analysis of ship based observations of wind speed and surface pressure by means of a boundary-layer model by Bumke and Hasse (1989). The derived SST were calibrated against those computed from Advanced Very High-Resolution Radiometer (AVHRR) data.

The evaporation fields were derived for individual over passes of the satellite during July 1983, with a spatial resolution of $1° \times 1°$. Evaporation cannot be directly measured and has to derived from other meteorological and oceanographic parameters. It was not practical to calculate the evaporation over the ocean via the most accurate methods, since large experimental effort was required, it was therefore decided to use the bulk aerodynamic method to calculate the latent heat flux. The problem, once again, was selecting as suitable value for the C_E coefficient. The value chosen was 1.2×10^{-3} without wind speed dependency, at least up to 18 $m.s^{-1}$. This value according to Crewell et al. was derived from the first results of the HEXOS experiment (see Glossary).

The bulk formula was applied to the actual data, not monthly means, of the individual parameters to compute the actual fields of latent heat flux, to avoid nonlinearity errors of the formulas. Because of the source of the data they were using they needed to derive SST, q_{10} and U_{10} (where $q_{10}$and U_{10} are the specific humidity and wind speed at 10m height . Their study showed that it is possible to calculate latent heat with an acceptable accuracy. It was calculated that the maximum error would be 60 $W.m^{-2}$ for individual measurements and 15 $W.m^{-2}$ for the monthly mean. These figures could be improved on if the computation of SST, q_{10} and U_{10} could be improved.

Most of the previous studies merely described the properties or spatial distribution of the climatological mean ocean surface heat fluxes, but little attention was given to the temporal variability. According to Cayan (1992c) a better knowledge of the variability would be important in the understanding of the ocean heat exchange process, which in turn is one of the key mechanisms in climate variations over a broad time-scale. Thus we see from modelling studies that air-sea fluxes are important mechanisms in ocean-atmosphere coupled models. In his study Cayan used bulk formula on four decades of surface marine data to examine the monthly variability in the sensible and latent heat fluxes over the global ocean.

Cayan found that in the extra-tropics the latent and sensible heat fluxes were strongly seasonal, with their maxima in the fall–to–winter when the thermal or vapour pressure contrast between the sea surface and overlying atmosphere

would be the greatest, as well as high wind speeds due to frequent storms. During these seasons latent and sensible heat fluxes dominate the net surface heat balance since solar heating is minimal and the net infrared radiation at the earths surface is relatively small. Cayan (1992c) also found that the anomalous variability of latent and sensible heat fluxes is also greatest during this fall–to–winter period, primarily because the mean wind, surface temperature and humidity contrast are greatest, and the weather and short-period climate variations largest.

Cayan used the bulk aerodynamic method because it is the only practical means of routinely calculating surface heat flux values over basin-scale regions. More exact methods, such as the eddy correlation method, require higher resolution data, and are only available in a few short lived process orientated experiments. On the other hand the routine marine weather measurements are available over broad sectors of the oceans for a period of several decades and provide the necessary data to compute the heat fluxes using the bulk formula.

Although recent estimates of the mean fluxes over the global oceans have been made, especially over the last two decades as briefly outlined above, an important feature of climate variability that has not been described is the temporal variability of the heat exchange between the ocean and atmosphere over a time scales of a month or longer. One of the reasons could be that " the heat fluxes are measured well enough to accurately close the heat budget for many large scale heat balance problems" (Blanc 1985). According to Cayan; Large and Pond (1982) noted that "accurate heat fluxes averaged over a few days are expected from the bulk method."

Cayan stated that spatially coherent anomaly variations of latent and sensible heat fluxes on monthly and longer time scales have been reported. Latent and sensible heat flux anomalies and local winds have been illustrated, and the connections of the anomalies of the El Niño–Southern Oscillation have been discussed. Cayan (1992c) examined the anomaly behaviour over a domain that included the region of the El Niño–Southern Oscillation and extended this work by investigating links to local and large-scale atmospheric variables.

Cayan (1992c) used the COADS (Comprehensive Ocean-Atmosphere Data Set) marine surface data set (Woodruff, Slutz, Jenne, and Steurer 1987). (See section 4.2.1 for full details.) The data set contains digitised, directly sensed surface marine weather reports, mostly observed from merchant ships. These variables include horizontal wind speed (w), horizontal wind vector components (u, v), sea-level pressure (P), specific humidity (q), relative humidity, air temperature (T), sea surface temperature and total cloudiness (C). Derived variables include the difference between SST and air temperature called δT, the surface saturation humidity and air humidity difference called δq, and the

products $w\delta T$ and $w\delta q$, the latter are monthly averages of the products of individual observations.

The particular data set used was the COADS "Monthly Summaries Trimmed" version, a 2° latitude-longitude gridded monthly average data set over the global ocean. Cayan used the data for the period 1946–1986. Cayan (1992c) notes that there is a greater density of observations in the middle latitude of the North Atlantic and North Pacific. The northern hemisphere contains a average of 66 000 observations per month for the years 1946–1986, in comparison with the southern hemisphere which has about 10 000. He also noted that there are slightly less $w\delta q$ samples than $w\delta T$, apparently because T and SST are measured more frequently than dew point or wet-bulb temperature.

In order to test the effect of different sampling densities the COADS Compressed Marine Reports (CMR) set was used in the Northern Atlantic. This consists of 10 years of well sampled 1° latitude-longitude "squares".

Using the observed and derived values from the COADS data set the latent and sensible heat fluxes were calculated using the following approximated form of the "sampling method" bulk aerodynamic equations:

$$F_l = \rho C_E \{w\delta q\} \tag{2.3}$$

$$F_s = \rho C_p C_H \{w\delta T\} \tag{2.4}$$

where:

F_l latent heat flux,

F_s sensible heat flux,

ρ density of air,

C_p specific heat of air,

L latent heat of vaporisation, taken as $2.50 \times 10^6 J.kg^{-1}$,

C_E transfer coefficients for latent heat,

C_H transfer coefficients for sensible heat,

w horizontal wind speed,

δq difference between the specific humidity at 10 metres and saturated specific humidity.

δT difference between the air temperature at 10 metres and the (sea) surface temperature.,

$\{\ldots\}$ products averaged over simultaneous pairs of individual observations for each month.,

Anomalies were constructed by subtraction of their long term monthly means. The data was also re-gridded into 5° squares because the primary interest concerns air-sea interaction over several hundred kilometres. Their spatial averaging also decreases random errors. This spatial averaging was applied to 2° anomalies to produce 5° anomalies. As for the value of C_E and C_H, Cayan (1992c) took them from Isemer and Hasse (1987, Table 4, p. 14) who used experimental evidence to derive the original Bunker (1976) values.

In order to understand the fluxes and their anomalies it is important to understand the *mean* fields of w and δq, w and δT. Each of the mean quantities is multiplied by the fluctuations of the other to produce the flux anomalies; in the case of latent heat anomaly:

$$F_l\prime \approx \overline{w}\delta q\prime + w\prime\overline{\delta q} \tag{2.5}$$

where the prime indicated the monthly anomaly and the overbar indicates the long term mean. Cayan asserts that this is a reasonable approximation as $w\prime$ and $\delta q\prime$ are not well correlated.

A zonal average measure was calculated from the standardised 5° product to provide an overview of seasonal and latitudinal dependence of the temporal variability of the monthly flux anomalies. To do this a zonal root mean square (RMS) of $\overline{\sigma}$ of the anomalies at individual grid points across each 5° latitude was defined as:

$$\overline{\sigma}(\zeta) = \left(\frac{1}{N_i} \sum_{j=1}^{N_i} \frac{1}{N_t} \sum_{t=1}^{N_t} \zeta_{ij}^2 \right)^{\frac{1}{2}} \tag{2.6}$$

where:

j one of the N_i grid points along a 5° latitude strip i;
ζ_{ij} is the monthly anomaly, of a particular variable, ζ sampled at month t
N_t is the total number of months.

The results are shown in the Table 2.1. Cayan, focusing on the northern hemisphere, noted that the maximum zonal RMS values occur within the period from October to March. (Which corresponds to the period of the largest mean and variability of w, δq and δT.) However, from table 2.1 it can be shown that the greatest variability in the fluxes are in the months April and July with a maximum of 35 $W.m^{-2}$ at 35° south in April, although there still is great variability in the latent heat flux all year: 18–35 $W.m^{-2}$. It is also clear that the variability of sensible heat flux (with

	Zonal RMS F_l				Zonal RMS F_s				Zonal RMS ($F_l + F_s$)			
Lat.	Jan.	Apr.	Jul.	Oct.	Jan.	Apr.	Jul.	Oct.	Jan.	Apr.	Jul.	Oct.
65°N			11				5				15	
60	40	21	9	23	32	13	4	14	68	32	11	35
55	34	16	8	24	31	10	3	11	62	23	10	34
50	33	17	8	23	29	9	4	9	60	26	10	31
45	33	17	9	23	23	8	3	8	52	24	10	30
40	41	21	13	25	21	9	2	7	61	30	15	31
35	41	24	12	25	16	7	2	5	56	30	13	30
30	36	19	13	24	11	3	2	4	44	22	14	27
25	29	23	15	24	7	4	2	3	34	26	16	26
20	31	22	14	22	4	3	2	3	33	24	15	22
15	31	20	19	20	4	3	3	3	33	22	20	20
10	25	20	19	18	3	3	2	2	27	22	20	19
5	17	19	20	18	2	2	3	2	18	21	22	19
0	14	16	17	18	2	2	3	3	15	17	19	20
5°S	18	19	19	18	3	3	3	4	21	20	21	21
10	21	25	27	20	3	3	4	4	23	24	30	23
15	20	26	29	21	3	4	5	4	22	28	32	23
20	20	23	22	18	3	4	4	4	20	25	24	20
25	18	27	23	22	3	4	4	4	19	29	26	25
30	30	27	28	22	3	5	7	5	19	33	32	23
35	31	35	31	23	6	7	8	7	32	37	36	28

Table 2.1: Zonal RMS F_l and F_S $W.m^{-2}$, from Cayan (1992)

a maximum of only 8 $W.m^{-2}$) is much less than that of latent heat flux. Cayan also noted that the largest anomalies occur in the western North Atlantic and North Pacific oceans, while in the Southern Hemisphere there seems to be very little seasonal variation at the 35 ° latitude. Finally Cayan stated that the Pacific ocean displays similar patterns in the spatial distribution of latent and sensible heat flux anomalies, however, there is a shift in the timing of the peaks in the Pacific, namely between October and December.

The primary objective of Cayan (1992c) study was to quantify the variance of latent and sensible heat flux.

Cayan (1992c) identified the degree to which each of the fundamental marine variables contributed to the anomalous variability of F_l and F_s. This was complicated by the fact that the fluxes are proportional to the products of these variables. This means that the average as well as the fluctuations of the fundamental variable are involved. Quantifying these contributions should provide a better understanding of synoptic and larger scale causes of the fluxes. In the analysis Cayan focused on the means and fluctuating components of w, δq or δT, C_E and C_H. The flux anomalies are also affected by air density, but since the variation through out the area of study is less than 5%, these are ignored. The latent heat flux is approximated by

$$\sigma^2_{F_l} \approx \overline{w^2 \delta q'^2} + \overline{\delta q^2 w'^2} + 2\overline{w}\,\overline{\delta q}(\overline{w'\delta q'}) \tag{2.7}$$

The variance of F_l denoted $\sigma^2_{F_L}$ is primarily controlled by the above three terms; which involve the product of $\overline{w}$ and $\delta q'$, the product of $\overline{\delta q}$ and w', and the $w'\delta q'$ covariance. $\sigma^2_{F_s}$ is described by a similar equations with δT substituted for δq. It was found that roughly equal contributions to $\sigma^2_{F_l}$ are made from $\overline{w}^2\overline{\delta q'^2} + \overline{\delta q}^2\overline{w'^2}$ terms, each accounting for about 40% of the total variance on average. Their geographical distribution is mapped in figure 2.1.

The covariance of w' and $\delta q'$ is weak and accounts for little latent flux variance. Nevertheless, the connection between w and δq is much richer than than the correlations reveal. Form a large scale perspective, both w and δq are organised by the atmospheric circulation.

In conclusion Cayan (1992c) noted that the magnitude and extent of the fluxes anomalies are important because these affect the heat content of the upper ocean and the heat and moisture content of the atmosphere, a coupling of the two must account for these variations of fluxes. The flux variations are greatest in the extra tropics and most variable in autumn and winter when seasonal heat stored in the ocean is released to the atmosphere. Since these anomalies are spatially coherent over fairly large regions and according to Cayan (1992c) they are linked to the monthly atmospheric circulation in both the North Atlantic and North Pacific; they therefore, contain a short-period "climate signal". Using empirical orthogonal functions (EOFs) it was shown that the first four EOFs summed accounted for about half the variance in each basin. The rotated EOFs represent regionally coherent anomaly packets. One reason for the spatial coherence is that rotated empirical orthogonal functions (REOFs) are related to sea level pressure, which in turn is influenced by monthly atmospheric circulation patterns.

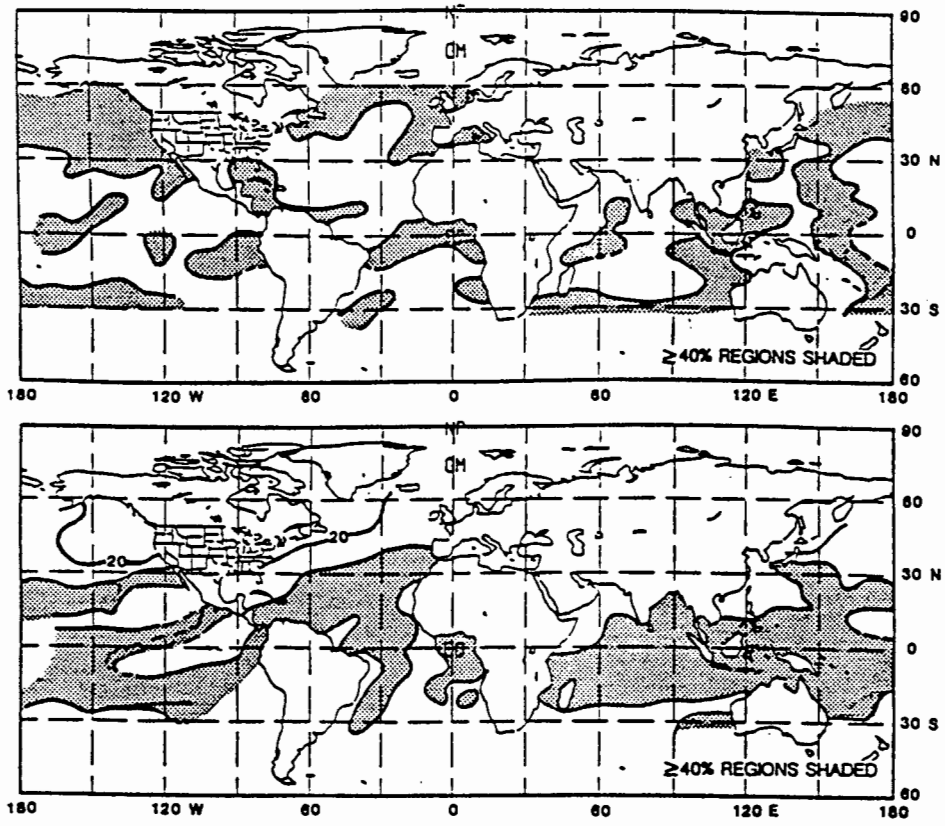

Figure 2.1: Fraction of F_l variance, $\sigma^2_{F_l}$, contributed by $\overline{w^2 \Delta q'^2}$ (above) and by $\overline{\Delta q}^2 \overline{w'^2}$ (below) computed from December, January and Feburary 1950–1986 data. Shaded areas indicated regions with greater that 40% variance explained. From Cayan (1992c)

2.2 Historical Calculation of Oceanic Heat Fluxes With Special Emphasis on Using The Bulk Aerodynamic Formulae And The Associated Problems

The bulk aerodynamic formulas were parameterised by Friehe and Schmitt (1976) using existing data and some new results. The coefficients were determined by performing least-square-error fits on the data. The following formulas were used by Friehe and Schmitt (1976) for the calculation of sensible and moisture fluxes:

$$H = \rho C_p C_H \overline{U}(\overline{T}_s - \overline{T}_a) \tag{2.8}$$

$$E = C_E \overline{U}(\overline{Q}_s - \overline{Q}_a) \tag{2.9}$$

where:

$\overline{U}$ = mean wind velocity (ms^{-1})

$\overline{T}_s$ = mean sea surface temperature (K)

$\overline{T}_a$ = mean potential air temperature (K)

$\overline{Q}_s$ = mean water vapour density (gm^{-1})

assuming the air to be saturated at dew point temperature

$\overline{Q}_a$ = mean water vapour density (gm^{-1}) at reference height

C_H = sensible heat transfer coefficient

C_E = moisture transfer coefficient

ρ = dry air density

Friehe and Schmitt (1976) determined that for moisture flux the transfer coefficient is 1.32×10^{-3}, Smith (1989) found that the coefficient is 1.2×10^{-3} for wind speeds less than 14 $m.s^{-1}$. However, Friehe and Schmitt could not determine a *single* transfer coefficient for sensible heat flux and so separate conditional formulas were developed. Even so, an approximate coefficient was determined, its value is $0.0012 + 1.41 \times 10^{-3}\overline{U}\Delta T$. Wu (1992) using the results of Friehe and Schmitt (1976) and Smith (1980) derived a set of transfer coefficients, one for stable conditions and one for unstable conditions. He notes that the coefficient has always been a constant for neutral atmospheric conditions. The two coefficient values are:

$(0.720 + 0.0175U_{10}\Delta T) \times 10^{-3}$ for $U_{10} < 8m.s^{-1}$

and

$(1.000 + 0.0015U_{10}\Delta T) \times 10^{-3}$ for $U_{10} > 8m.s^{-1}$

Esbensen and Reynolds (1981) showed that one of the major problems with the work of Bunker (1976) that while it is possible to calculate oceanic heat flux from individual observations and average, that more than 30 million ship reports would need to be processed to obtain the sensible and latent heat flux values. The main purpose of their paper was to provide a basis for determining to what extent the classical method of calculating fluxes of sensible and latent heat from monthly averaged meteorological variables can be used for studies on the order of interannual and decadal climatic variability. The classical method uses equations 2.8 and 2.9 whereas the sampling method uses the following equations (these are the same formulas Bunker (1976) used for his calculations.):

$$H_s = \rho C_p \overline{C_H U (T_s - T_a)} \tag{2.10}$$

$$E_s = \overline{C_E U(Q_s - Q_a)} \tag{2.11}$$

where:

U = wind velocity (ms^{-1})

T_s = sea surface temperature (K)

T_a = potential air temperature (K)

Q_s = water vapour density $(g.m^{-1})$
assuming the air to be saturated at dew point temperature

Q_a = water vapour density $(g.m^{-1})$ at reference height

C_H = sensible heat transfer coefficient

C_E = moisture transfer coefficient

ρ = dry air density

overbar = average.

Rather than using completely empirical methods for determining the transfer coefficients of equations 2.8 and 2.9 Esbensen and Reynolds (1981) used boundary-layer similarity theory which provides a rational, physical basis to minimise the dependence of C_H and C_E on empiricism. One advantage of similarity theory is that it allows the inclusion of the effects of atmospheric boundary-layer, with the measure of stability being the Monin-Obukhov length L which is defined as:

$$L = \frac{(\tau/\rho)^{2/3}}{g\overline{T}_v^{-1}\overline{w'T'_v}} \tag{2.12}$$

where:

τ = is the magnitude of the surface wind stress,

T_v = is the virtual temperature and

g = gravitational acceleration.

$\overline{w'T'_v}$ = The overbar indicates the Reynolds averaging of the product where:

w = is the vertical air velocity.

Using three-hourly observations, from nine ocean weather ships, over a 25 year period (1948–1972) latent and sensible heat flux were calculated using both the classical and sample method. By comparing these two results

Esbensen and Reynolds showed that by using monthly averaged wind speed; temperature and humidity, latent and sensible heat flux can be calculated by the classical method to within a 10% relative error. Since, according to Esbensen and Reynolds (1981), the transfer coefficients are subject to uncertainties of 20%–30% the classical method can be considered a practical and reliable alternative to the sampling method. Furthermore, the results suggested that the classical method was successful in monitoring interannual variability. These calculations were done both for the winter and summer months as well as for the mid-latitude and sub-tropical regions.

Grachev and Pannin (1984) found that under certain weather conditions the bulk aerodynamic method fails ($u < 3m.s^{-1}$) and ($u > 15m.s^{-1}$). For moderate conditions, with wind speeds of 3–15 $m.s^{-1}$yields satisfactory results. They suggest using different formulas, such as adding a term that is not dependent on the wind speed.

Blanc (1985) using ten published bulk aerodynamic formula transfer coefficients schemes and more than 2600 sets of shipboard data over one year calculated, using the same data with different schemes, fluxes of latent heat flux, sensible heat flux and momentum flux at Ocean Station C in the North Atlantic, located midway between Newfoundland and Ireland at 55 ° 45 'N, 35 ° 30 'W. Of the twenty or so bulk transfer schemes, or combination of schemes there is no universally accepted scheme. The schemes vary in complexity, from the Friehe and Schmitt (1976) scheme which uses the statistical averaging of many experiments to schemes which use stability dependent coefficients for example. Each of the ten schemes were chosen as being representative of the various classes of a combination of schemes presented in the then recent literature. As mentioned before, the bulk method is least reliable at either end of the wind or stability scales due to the relative lack of data taken during experiments which lead to the development of the transfer coefficient schemes. Over the one year period, Blanc (1985) found that the mean parameter magnitudes were 25 $W.m^{-2}$ for sensible heat flux and 40 $W.m^{-2}$ for latent heat flux. Unfortunately (according to Blanc 1985) there is no way of knowing which of these bulk schemes, if any, are correct. There is a need for more accurate measurement in a wide variety of atmospheric and oceanic conditions. Of the ten schemes used, many were taken in the equatorial regions of the Atlantic Ocean, under stable conditions and wind speeds less that 15 $m.s^{-1}$. Blanc (1985) stated that although his paper emphasised the serious problem that exists with the bulk method, there is no alternative than to use this method. He concluded by stating that we may have already reached the accuracy limitation of the bulk method because of the simplicity of the method's underlying assumptions and it may be unrealistic to expect greater that a $\pm$ 50 % accuracy in the fluxes.

According to Hsiung (1986) the basic errors in heat flux calculation by the Bulk Aerodynamic Method can be grouped into two categories: systematic errors and random errors. The main sources of the first are the inadequacy of the bulk aerodynamic formulas as an approximation of the true fluxes, bias arising from inadequate data sampling both spatially and temporally.

However, the amount of uncertainty of calculation associated with the bulk formulas is difficult to assess because there is a lack of verification of fluxes calculated by other means over the open oceans. In addition to this problem, ship's data often does not provide sufficient data over the lower atmosphere or upper ocean to calculate the fluxes. A major problem is the calculation of the transfer coefficients, which is especially important for latent heat flux as it is one of the most important components of the total heat budget. Cayan (1992c) commenting on the COADS data set, notes a linear increase in mean wind speed of 0.8 $m.s^{-1}$ over the years 1950–1986. This is probably artificial, involving changes from the Beaufort Scale to anemometer observations. Both δT (the difference between the air and sea surface temperature) and δq (the difference between the saturated specific humidity and specific humidity) vary: the former by about 0.2° C over 1950–1986, the latter is not spatially coherent and varies both positively and negatively.

Random errors occur mainly from non uniform observation techniques, reporting and archiving methods. For example Hsiung (1986) uses latent heat flux, since C_E is a function of wind speed and therefore errors in wind speed would give different values in the flux calculation. It is presumed these errors are random and will decrease with increasing observations. Averaging over large time and space scales reduces this type of error. Cayan (1992c) noted that ideally monthly heat flux estimates would only contain short-term climate fluctuations with periods of two months and longer. Using a Monte Carlo simulation to generate random errors it was calculated that the error in the flux calculation was less than 10 $W.m^{-2}$ for F_l (equation 2.3)and less than 5 $W.m^{-2}$ for F_s (equation 2.4), for 100 "observations".

Blanc (1987) discussed the problems associated with various bulk method determined fluxes and the difficulty of making these measurements over the ocean. Blanc concluded that there are four main principle sources of errors made in the bulk aerodynamic flux calculation, using ship data. These are summarised as follows:

- the accuracy of the flux measurements used to develop the bulk method;
- variations from different bulk aerodynamic schemes;

- the accuracy of the various meteorological sensors used and
- the errors induced by the presence of the ship itself.

In previous studies (Blanc) showed firstly that, with a few exceptions, most experiments used the profile method as a basis for the bulk aerodynamic method. This can lead to errors of between 15% to 105 % for fluxes in the range 5–150 $W.m^{-2}$ and 10–300 $W.m^{-2}$ for sensible and latent heat respectively. Secondly, because of the different transfer coefficient schemes a variation of 15 % to 30 % occurs in the fluxes. Thirdly errors are induced by sensor inaccuracies, these are usually compounded when more than one sensor is used in collecting the necessary meteorological data. Errors from these sensors result in an uncertainty of 10 % to 155% for the fluxes. Fourthly, the actual ship can seriously distort the meteorological reading, the ships hull and superstructure induce distortions in the wind speed, air temperature and humidity. Blanc (1987) noted that in some experiments a higher than 2° C increase in air temperature due to the heating influence of the ship during the day. On average these effects account for 15% to 115% of the uncertainty in the heat fluxes. Blanc (1987) assumed that these four principle sources of uncertainty were independent and were combined, to determine the most probable overall influence. When combined the cumulative effect is that for sensible heat flux between 5–150 $W.m^{-2}$ the overall accuracy is between 35–220 %; for latent heat flux between 10–300 $W.m^{-2}$ the overall accuracy is between 40–125 %. For sensible heat flux the majority of the uncertainty below 60 $W.m^{-2}$ is due to sensor inaccuracy and ship distortion, for 60–150 $W.m^{-2}$ it is probably due principally to the coefficients used. For latent heat flux less that 200 $W.m^{-2}$ the main uncertainty is basis accuracy (with a few notable exceptions, most experiments used to develop the bulk method used the profile-derived method as a basis which itself is not totally accurate), and for values between 200–300 $W.m^{-2}$ the coefficient scheme used.

Weare and Strub (1981) showed, using two different regions in the Pacific, that assuming the data is equally distributed both spatially and temporally throughout a 5° block and the area is free of tropical storms, that the minimum number of observations needed to assure the accuracy of individual monthly latent and sensible heat fluxes was eleven.

Ruprecht and Simmer (1991) conducted a review of different methods of calculating latent heat flux over the oceans, with special emphasis on the bulk aerodynamic method. They stated that when looking at general circulation and climatic process the flux of water vapour is the most important of all fluxes, and water vapour flux or evaporation stands out above all other vertical fluxes. Together with water vapour flux, a significant amount of energy in the form of latent heat is transfered, to the atmosphere. (Hence water vapour flux and latent heat flux are often used

interchangeably although their units are different, $kg.s^{-2}.m^{-2}$ and $W.m^{-2}$ respectively.) Latent heat is the main source of energy for many processes in the atmosphere, especially in the tropics. According to Ruprecht and Simmer (1991) on a global average each atmospheric column receives approximately 240 $W.m^{-2}$ directly from the sun; with an average rainfall of 1 m per year (equal to the average evaporation) the same column receives 80 $W.m^{-2}$ from the release of latent heat. However, since rainfall is concentrated in small areas, the importance of the hydrological cycle, which starts with evaporation at the earth surface, particularly over the oceans, is easily understood for many processes in the atmosphere.

The problem with quantifying evaporation is that it is that not a measurable parameter, but rather derived. At time of writing (Ruprecht and Simmer 1991) stated there are four methods of calculating water vapour flux:

1. eddy correlation method,
2. profile method,
3. dissipation method,
4. bulk aerodynamic method.

Of these the first is an almost a direct measure of evaporation and is often used as a calibration for the other methods, but it is very difficult to calculate evaporation using this method as it requires precise measurement of both atmospheric and oceanographic variables. The second and third methods require higher technical effort, such as the measuring of vertical velocity at high frequencies ($>$ 1 Hz). The differences between the methods of calculation lead to different determinations of water vapour flux, when applied to the same data. Blanc (1987) showed that the last three methods which are indirect methods, produce the following differences in the water fluxes

1. The eddy correlation against profile method , $<$ 25 %;
   the dissipation method , $<$ 40 % ;
   the bulk aerodynamic method, $<$ 55 %.
2. Eddy correlation method, at the same location and time but different instrumentation, $<$ 10 %.

To determine large scale or even global fields of evaporation only the bulk aerodynamic method can be used because it needs meteorological parameters only. It is possible to determine these parameters from satellite observations and

this makes its possible to calculate water vapour flux over vast oceanic areas where more conventional observations are not available.

2.3 Fluxes And Their Influence On Weather and Climate

Namias and Cayan (1981) stated that it has been shown that there is order in large scale air-sea interactions, so large scale abnormalities of the lower atmosphere and the upper ocean thermal structure are comparable. The patterns in the ocean are approximately an order of magnitude more persistent than the atmospheric circulations. The problem that exists is that the mechanisms which produce these large scale oceanic features are not well known.

Hastenrath and Lamb (1980) studied the heat budget of the Indian Ocean. They examined both the hydrosphere and atmosphere with a view to describing the regional and annual variations. They investigated the sensible and latent heat fluxes and linked these to the monsoon. They concluded the southern tropical Indian Ocean appears to provide the major moisture supply for the monsoon.

The question that arises is, "Is there any relationship between monthly mean precipitable water and surface level humidity?" Liu (1986) using data from 49 ocean stations, islands and ships over a period of 17 years showed a statistical relationship between monthly-mean precipitable water (W) and mean-monthly surface-level mixing ratio(Q). It was found that this relationship holds for all the major oceans and can be used effectively to monitor interannual variability.

The world's oceans were divided into four regions: North Pacific, South Pacific, Indian and Atlantic. Scatter-plots of W versus Q were plotted and a fifth-order polynomial constrained to pass through the origin was fitted. According to Liu it was apparent that this relation held in both the Southern and Northern hemispheres and in all ocean basins. In general there is no systematic difference between summer and winter months with respect to this relationship. An interesting observation is that in an area that has W below 4.5 $g.cm^{-2}$ the area is characterised by a higher Q to W ratio, indicating that the moisture is kept more at the surface. On the contrary a small change in Q corresponds to a relatively large change in W above this level.

Leslie, Holland, and Lynch (1987) using the Bureau of Meteorology Research Centre (BMRC) limited-area model described a total of eleven numerical atmospheric circulation simulations they ran. These were exploring the ability of

the model to forecast cyclogenesis. In two of their experiments they looked at the effect of surface fluxes on cyclogenesis, they found that there was a strong coupling between boundary layer fluxes of heat and moisture and the initiation of convection. They also stated that surface conditions are important contributors to cyclone development, since the effects of zeroing all surface fluxes and frictional dissipation resulted the cyclone track been very poorly predicted. The preliminary conclusion was that the convective release of latent heat is important to cyclone development.

Atlas (1987) examined the role of oceanic fluxes in the numerical prediction of an intense coastal storm. Using the storm of 18–19 February 1979, known as the President's Day cyclone, the failure of the U.S. National Meteorological Centre (NMC) model to predict this storm created great interest. Atlas (1987) presented the results from the Goddard Laboratory for Atmospheres (GLA) model predictions as well as the importance of air-sea interactions. A number of experiments were run on the GLA model, the first with no restrictions, a second without sensible and latent heat fluxes and a third without moisture flux.

The first experiment yielded good results with the model accurately forecasting the track of the cyclone, but due to an initial overestimate, the cyclone became progressively slow with time. The second and third experiments show no cyclonic development along the coast. In analysing these results Atlas (1987) found that that very strong fluxes of heat and moisture from the ocean to atmosphere are present in the first 24 hours of the prediction, and although weaker, also significantly present in the next 24 hour period. These fluxes contribute to a substantial warming of the atmosphere and increased baroclinicity. In comparison, forecasts without the surface sensible and latent heat flux show a significant increase in upper level gradient of vorticity, vorticity advection and divergence. Atlas (1987) concluded that diabatic heating resulting from oceanic fluxes significantly contributes to low level cyclonic vorticity, increased baroclinicity, decreased static stability and intensification and slow rate of movement of an upper level ridge. These factors resulted in the GLA model effectively forecasting the cyclone where the NMC model had failed.

Having established that surface oceanic fluxes are important Reed, Simmons, Albright, and Undèn (1988) examined the role of latent heat release in explosive cyclogenesis using the predictions of the ECMWF model. They looked at a particular case study, a one week period in January 1986 in which three such events occurred. The first two were well predicted by the model, however, the third was not. The question they wanted answered was how much of the deepening results from dry baraclinity alone, and how much from the release of latent heat? To answer these questions the model was rerun with the latent heat released during condensation not allowed to warm the atmosphere. In the first case the latent heat release accounted for 46 % of the deepening and in the second case 41 %. In the case that

was poorly forecast, latent heat release accounted for only 33 % of the deepening.

Reed, Simmons, Albright, and Undèn (1988) concluded that in the two examples of strong rapid cyclogenesis that were predicted by the ECMWF T106 model, latent heat was found to account for 40–50% of the deepening. The results of the third case were less successful and attempts to determine the cause(s) were inconclusive.

Lambert and Boer (1989) considered twelve atmospheric GCM's and looked at the atmosphere-ocean heat fluxes and stresses in these models. They found that although most uncoupled GCM's develop ocean atmosphere fluxes quantitatively similar to those of a climatological estimates there are considerable differences for some models and great variation between models. This highlights two possible errors: the existence of a systematic model error and lack of good observation-based knowledge. To improve these GCM models both of these areas need to be improved. Palmer, Branković, Molteni, and Tibaldi (1990) made a set of 30–day integrations with the ECMWF model over a period of three and a half years (1985–1988). They looked at the impact of the model reformulation over this period, and they found that the improvements had effected among other things the eddy fluxes of both heat and momentum.

Miller, Beljaars, and Palmer (1992) carried out a series of simulated experiments, with the ECMWF forecast model, to examine the model's parameterisation of evaporation from the tropical oceans. As noted by Miller et al. (1992) SST variations modulate the convective activity, and hence the diabatic forcing, this happens through the evaporation from the ocean surface. Therefore correct parameterisation of the GCM's boundary–layer processes, including surface latent heat flux, is critical. Moisture for convection comes from a combination of local evaporation and advection from more remote areas. Miller et al. examined the area of the tropics characterised by high, largely uniform SST and low wind speeds.

Simonot and Treut (1987) used the ECWMF model surface heat fluxes over a twenty two month period. The main problem was that the models annual net sea surface flux was 40 $W.m^{-2}$ and therefore not in equilibrium. The latent heat flux loss of 28 $W.m^{-2}$ corresponds to loss by evaporation of $1mm.day^{-1}$. The bias that is seen could be explained by the absence of shallow convection from the model during the 22 month period.

In the ECMWF model the evaporation is parameterised in the following form:

$$-\frac{E}{\rho} = C_Q \mid U \mid (q_1 - q_s) \tag{2.13}$$

where:

E = evaporation,

ρ = air density,

C_Q = transfer coefficient for moisture,

U = horizontal velocity of the lowest model level,

q_1 = specific humidity at the lowest model level and

q_s = specific humidity at the surface (saturation value at SST)

The problem with this equation is that the terms used to calculate C_Q underestimate the stability correction and do not account for smooth surface scaling at low wind speeds. The problem is compounded by the fact that at low wind speeds, below 5 $m.s^{-1}$, hardly any data exists, but it is felt that the evaporation cannot be less that the evaporation from an areodynamically smooth surface for which the transfer properties are well established from laboratory experiments. Equation 2.13 is modified to the following:

$$-\frac{E}{\rho} = C_Q\{\mid U \mid^2 + w_*^2\}^{\frac{1}{2}}(q_1 - q_s) \tag{2.14}$$

$$w_* = \left\{-z_i g\frac{\overline{\rho' w'}}{\rho}\right\}^{\frac{1}{3}} \tag{2.15}$$

Where:

$g\frac{\overline{\rho' w'}}{\rho}$ is the buoyancy flux at the surface.

z_i is the boundary–layer height

For low wind speeds the new scheme enhances the evaporation, and for strong winds the flux is reduced.

Using this new formula, experiments were carried out by Miller, Beljaars, and Palmer (1992) on the ECMWF model during summer and winter. The increase in evaporation over quite large areas of the tropical oceans, especially over the warm pools were found to be on the order of 25-50 $W.m^{-2}$. Miller et al. (1992) stated that tropical circulation is extremely sensitive to apparently minor changes in the way evaporation is parameterised. By increasing the latent heat flux at low wind speeds by no more than 25 $W.m^{-2}$ there is a major improvement in the systematic errors of wind and temperature, and in rainfall patterns.

Gordon and Hunt (1991) sought to develop a deterministic drought prediction scheme, using a GCM to simulate rainfall perturbations by SST anomalies in the Pacific Ocean. The GCM model was run with a fixed January mode with three SST anomalies patterns, representing the El Niño, anti-El Niño and a control run. It was found that reasonable rainfall perturbations occur with the varying input parameters. Time series plots of the condensation heating level of the models troposphere show that there is no simple relationship between the imposed SST anomalies and the consequent release of latent heat in the atmosphere.

Cayan (1992a) tested part of the ocean surface heat budget by relating monthly anomalies to the latent and sensible heat fluxes to anomalous tendencies in SST field. There was ample evidence for significant anomalies of latent and sensible fluxes over the "weather" to short-period climate range. It was noted that in mid-latitudes, the largest latent and sensible heat flux occur in cold sectors of storms, where significant monthly and interannual variations occur. The equatorial latent heat flux anomalies were systematically related to the El Niño–Southern Oscillation (Cayan 1992a).

Cayan (1992a) examined the anomalous variability of the bulk formulas of latent and sensible heat flux. Because these two fluxes are strongly correlated they were considered as a sum and they were calculated from the COADS data set (see page 12). Broadly speaking it was found that Q_H increased poleward of 35° . This is due mainly to the fact that the term $\overline{w}\delta T$ becomes larger. It was also found that the Q_l anomalies dominate from 10° N to 30° S. Cayan (1992a) found that the heat flux anomalies are consistent over large areas with both atmospheric circulation anomalies and with month–to–month changes in SST anomalies. The monthly flux anomalies and SST anomalies are correlated over much of the oceans, with anomalous positive/negative fluxes associated with anomalous cooling/warming. This correlation is strongest in the extra-tropics during the cool season when the latent and sensible fluxes and their variability are greatest, and the radiative fluxes weakest.

Cayan (1992c) stated that while the heat flux forcing of the SST anomalies operates locally, the flux and SST tendency anomalies are organised over large spatial scales often spanning major portions of the North Atlantic and North Pacific. Using canonical correlations, it was shown that large-scale, co-located anomaly patterns occur in both regions. Typical fluxes of $50W.m^{-2}$ are associated with changes of order 0.2° C.

Cayan (1992b) further examined the relationship between atmospheric circulation and monthly anomalies of ocean surface latent and sensible heat flux. It was found that in the Northern Atlantic and Northern Pacific (north of 15°) that the flux anomalies were partially caused by local variations in the monthly mean wind direction. Large

positive anomalies occur during northerly and northwesterly winds, in the extra-tropics, in response to the advection of humidity and temperature form north to south. In contrast to the tropics, there in little significant correlation because of the weak gradients of humidity and a relatively steady wind direction.

Cayan (1992b) found that the most significant connection between the wind and flux anomalies is located on the basin scale, and associated with monthly atmospheric circulation. Using EOF, on sea level pressure anomalies it was found that the dominant atmospheric modes have systematic patterns of anomalies in wind speed, surface saturation humidity–air humidity difference, (δq) and SST–air temperature difference (δT). These together produce large scale patterns of latent and sensible heat fluxes. In the extra-tropics major negative SLP anomalies tend to have positive w anomalies to its south and negative w to the north, while δq(and δT) anomalies lie to the west and east of the low. This is apparently caused by the meridional air advection, which the SLP centres, with enhanced sea to air fluxes to the southwest of the center and results in the flux anomalies shifted meridionally and zonally about diminished fluxes to the east of the anomalous low. Areas of increased monthly flux also tend to have larger than normal intra-monthly variability in the fluxes. Months with strong monthly atmospheric circulation anomalies frequently exhibit combined latent and sensible flux anomalies with magnitude exceeding 50 $W.m^{-2}$ over regions of the order of several hundred kilometre regions.

Chapter 3

Variation of South African Summer Rainfall

In this chapter we consider summer rainfall patterns as well as some of the mechanisms that are of direct concern to South African rainfall variability and distribution. In this context we discuss in particular the main rain bearing systems in the South African Summer rainfall region. This is primarily done by reviewing the work of Harrison (1984). Once we have identified the main rain bearing systems we examine the effects of the Southern Oscillation on the rainfall patterns. This is done so that we exclude the effects of the Southern Oscillation on the rainfall distribution. Similarly, we examine the work of Walker (1990) who studied the effects of SST on rainfall. Using these ideas as a basis we then look at the effects that latent heat flux has on the summer rainfall patterns.

3.1 The Synoptic Climatology Of South Africa

In this section we look at the work of Harrison (1984) and his development of a synoptic classification system, so that we can determine which is the most important rain bearing system in the summer rainfall region. Earlier Tyson (1984) showed that 30 % of the variance in annual rainfall over South Africa can be accounted for by quasi-periodicities of the order of 18 to 21 years. Tyson's work led to the estimation of future rainfall trends in ten year cycles.

South Africa's seasonal rainfall areas can be classified into three main types:

- The Summer Rainfall Region: located mainly in the Transvaal, Orange Free State and Northern Cape; receives most of its rainfall during the summer months.
- The Winter Rainfall Region: located over the South Western Cape; receives most of its rainfall during the winter months.
- The Perennial Rainfall Region: along the southern coast of the Cape Province; receives its rainfall throughout the year.

The summer rainfall region encompasses the largest area of South Africa in comparison to the other rainfall regions. The importance of the summer rainfall region is the high population density and associated intense agriculture. Improved prediction of rainfall in this region is critical for economic and agricultural reasons.

This chapter, and indeed the dissertation concentrates on the summer rainfall region, because of the huge impact this region has on the entire country, in terms of the economy and food production.

A classification of South African summer rain-bearing synoptic systems was undertaken by Harrison (1984) using *S-mode Principal Component Analysis* (PCA) of standardised monthly rainfall and METEOSAT imagery. Harrison (1984) considered the monthly rainfall for a period of 57 years, from 1921 to 1977 over the eight summer southern hemisphere months, September — April. Using PCA Harrison reduced the data to eight sets of fourteen spatially dependent time series which together accounted for 90 % of the rainfall variance of the original series. Harrison (1984) postulated as an hypothesis that acceptable *physical* interpretations could be made from the the purely mathematical calculations of PCA.

In an earlier study of a "2° × 2° " block in the Orange Free State, Harrison (1983) demonstrated that monthly rainfall totals were statistically linked to the frequency of rainy days alone. Harrison assumed that this relationship holds throughout the country, this means that for a first approximation the amount of rainfall is related to the number of times a particular, relevant atmospheric circulation system moves over the area. By using PCA; an increase in the frequency of a certain system passing over a particular area will be reflected both in rainfall and in the eigenvector describing the relevant pattern. These eigenvectors are hypothesised to be linked with a particular synoptic system. Polar orbiting satellite imagery was used to identify these systems during unusually high or low values of the eigenvector corresponding to increased or decreased frequency of systems whose rainfall pattern matches the magnitude of

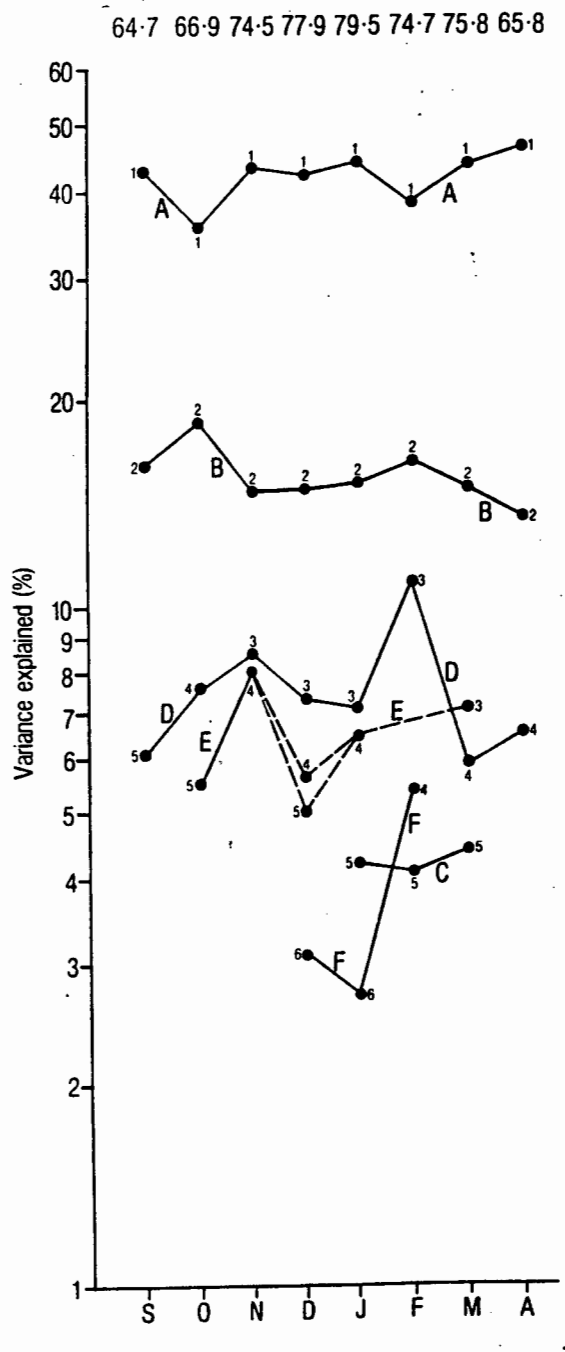

Figure 3.1: Variance (in percent) explained by each component. From Harrison, 1984

the eigenvector or the loadings field of the eigenvector.

For example each component that corresponds to some given components of similar physical interpretations are

then linked together and given an identifying letter. The results shown in figure 3.1 demonstrate that component A dominates from September to April and this explains in excess of 35 % of the total variance in all months. Components A and B together explain close to 60 % of the total variation in all months (figure 3.1).

Both components A and B were linked to tropical-temperate troughs. Harrison (1986) concluded that tropical-temperate troughs with their associated cloud bands connecting the tropical cloud masses to temperate cyclones are the most important contributors to rainfall over the interior of the country. Subtropical cyclones also contribute to rainfall over the interior of the subcontinent. These two systems thus account for the majority of the rainfall in the summer rainfall area. In figure 3.2 these systems are marked 'a' and 'b'.

Harrison suggested that monthly rainfall totals over the central interior of South Africa increase with enhanced poleward momentum fluxes across the Southern African subcontinent. These temperate-tropical troughs form an interaction between the tropical and temperate circulations. These temperate-tropical troughs mark a channel for poleward export by the mean meridional circulation of momentum and energy generated along the Inter Tropical Convergence Zone (ITCZ). These troughs develop mainly in January when the ITCZ is furthest south. Momentum and energy generation over Africa in the vicinity of 20° appears to be a necessary condition for the formation of tropical-temperate troughs (Pathack 1993). Harrison concluded that such a classification system facilitates interpretation of the rainfall variations over the summer rainfall region of South Africa in terms of the accompanying atmospheric circulation patterns in a manner not previously described.

3.2 The Effect of The Southern Oscillation On Atmospheric Circulation

In this section the work of Lindesay (1988a) and in particular the influence of the Southern Oscillation (SO) on atmospheric circulation and rainfall patterns has been considered.

Research carried out on general circulation mechanisms of non-seasonal and other climatic variations have focused on teleconnections with the Southern Oscillation which is a major mode in southern hemisphere atmospheric variability (Lindesay 1988a). These effects, however, are not new, the Southern Oscillation was first identified at the turn of the century by Hildebrandsson (1897) and Lockyer and Lockyer (1902) and later Walker (1923) described this phenomenon as "... a swaying of pressure on a big scale backwards and forwards between the Indian Ocean

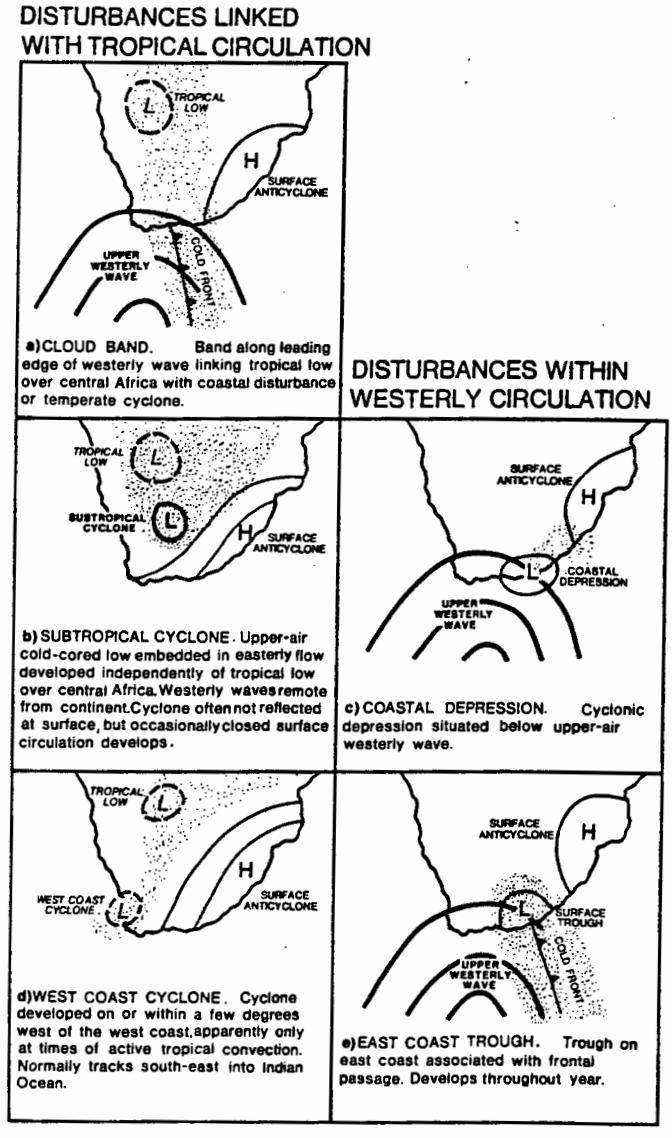

Figure 3.2: Generalised classification of major seasonal rain-bearing synoptic systems over South Africa. Stippled areas suggest typical cloud distributions. Lower troposphere circulation features are suggested by thin, full lines, upper troposphere features by thick, full lines and features present throughout most of the troposphere by dashed lines. From Harrison, 1984

and Pacific Ocean ..." (Walker, 1923, p109). It was Walker (1924) that gave this phenomenon the same "Southern Oscillation". Extensive research has followed, with investigators searching for a precursor to the Indian monsoon. Berlage (1957, 1966) and produced a correlation map of surface pressure and from this defined two centres of action

for the Southern Oscillation. The correlation in the surface pressure showed a maximum of -0.8 between two centres, one around the Indonesian region and the other over the Eastern South Pacific. In short, the Southern Oscillation can be described as the oscillation of pressure (mass) between these two centres. When in the high phase there are cold eastern Pacific Sea Surface Temperature (SST) and a strong South Pacific Anticyclone. In the low phase the reverse anomalies hold. The change form one mode to the next is aperiodic, but has a variation between 2 and 10 years.

The Southern Oscillation is also linked with another phenomenon, that of the El Niño. The El Niño manifests through a warming of waters across the eastern Pacific and the coastal waters of South America. The composite of these two features, ocean and atmospheric, is known as the El Niño-Southern Oscillation (ENSO) (Philander 1983). A common measure of the Southern Oscillation Index (SOI) shown in figure 3.3 is the standardised monthly sea-surface pressure difference between Tahiti (17.5° S, 149.6 ° W) and Darwin (12.4° S, 130.9° E); a high phase of the Southern Oscillation is marked by a higher than normal pressure at Tahiti and vice versa.

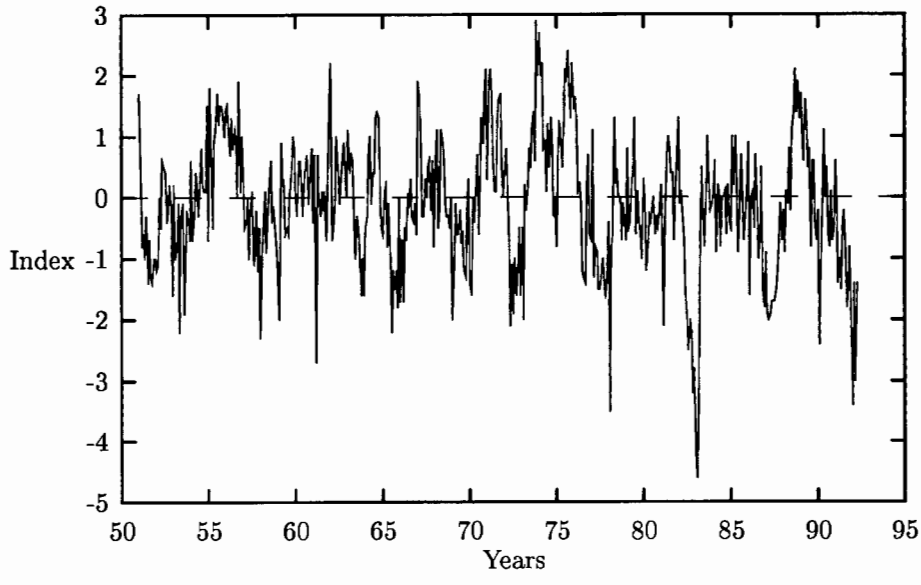

Figure 3.3: Southern Oscillation Index from 1951 to 1992

Lindesay (1988a) made a detailed study of the Southern Oscillation and its relationship, amongst other things, with the variability of South African rainfall. Using monthly data from 60 rainfall stations and grouping them 3-monthly, an index was computed for the months October—December, January—March, April—June and July—September

for the period January 1935 to September 1983. Both monthly and seasonal rainfall series were correlated with the corresponding Southern Oscillation Index at zero lag.

The results indicated that during the early summer months, October and November, there was poor correlation and the spatial distribution lacked coherence. However, for the late summer months, December to February, the correlations were characterised by spatially coherent areas and high correlation values. In December when correlations exceeded 0.45, these values are statistically significant at higher than 99 % confidence level. An inverse of this was found in the south western Cape. Figure 3.4 illustrates the north-west to south-east orientation zone of relatively

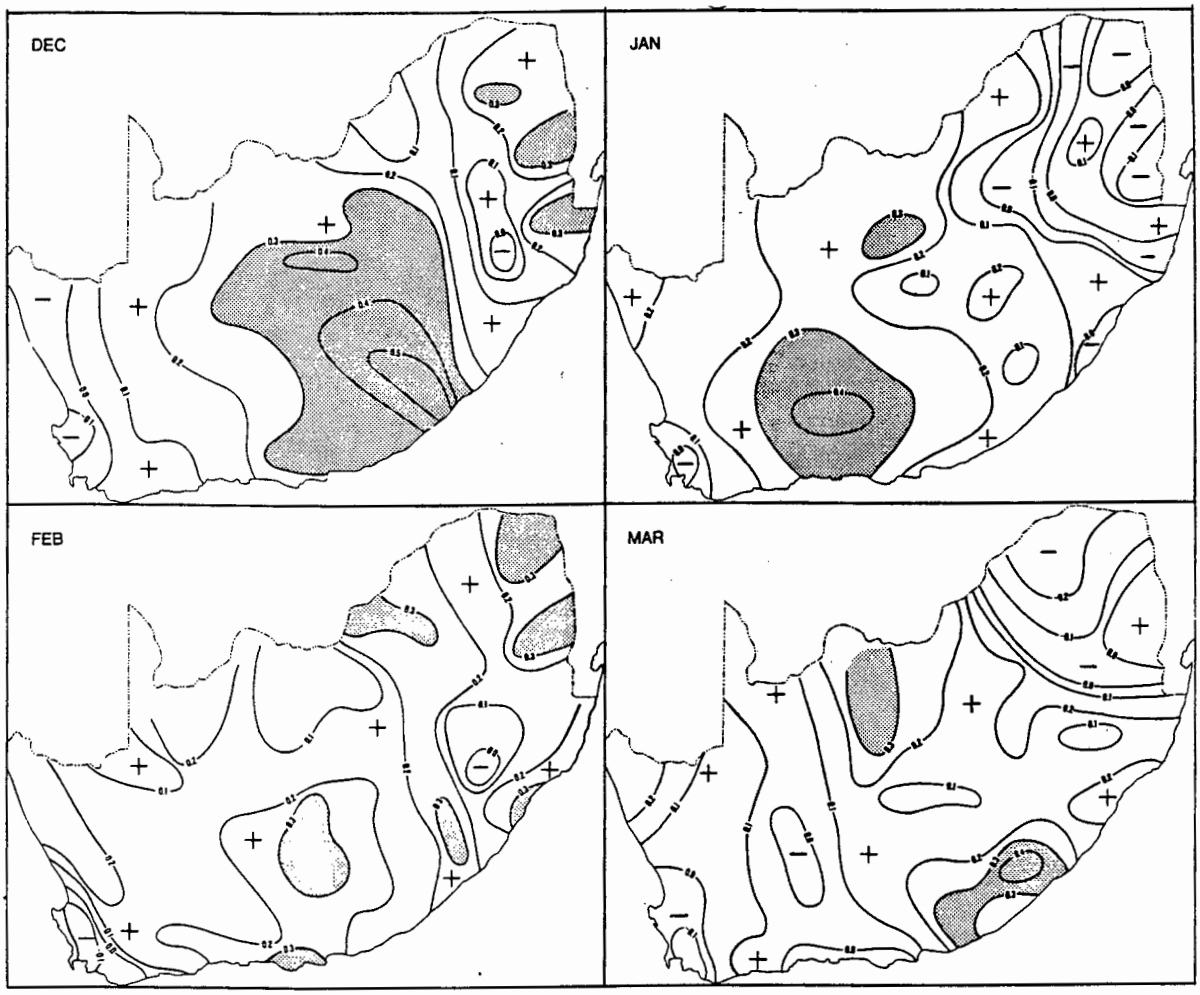

Figure 3.4: Fields of correlation between monthly station rainfall series and the Southern Oscillation Index. Shading represents areas of greater than 5 % confidence level. From Lindesay, 1988.

high positive correlation is present in the months of December to March. This feature is probably linked to the

tropical-temperate troughs mentioned in section 3.1 (Pathack, Jury, Shillington, and Courtney 1993). Harrison (1986) suggested that the Southern Oscillation modulates variations in the frequency and preference in location of major cloud bands which contribute to a large proportion of the summer rainfall over the country.

Simultaneous variations in the Southern Oscillation Index with rainfall account for 20 % of rainfall variance over South Africa. The relationship is such that high rainfall tends to coincide with the high phase of the Southern Oscillation and vice versa. However these relationships are not stable in time. Spectral analysis and lagged correlations were carried out on this data, but failed to yield any noteworthy results. The rather erratic nature of the Southern Oscillation limits its use as a predictor of rainfall on annual time scales. Not with standing this, Pathack et al. (1993) remarked that the close relationship between Southern Oscillation Index spectra and South African rainfall at both quasi-biennial and Southern Oscillations periods (2 to 10 years) support the physical mechanism linking phase changes of the Southern Oscillation with zonal and meridional circulation adjustments over Southern Africa, and therefore with rainfall over central parts of South Africa.

3.3 Variation of Summer South African Rainfall With SST.

Walker (1990) undertook a study to investigate the link between the summer rainfall variability in the summer rainfall region of South Africa and sea surface temperature (SST). The rainfall data set used in the study was compiled by Lindesay (1988b) and obtained from the Climate Research Group at the University of Witwatersrand. The SST data set was collated from the VOS data set obtained from the United Kingdom Meteorological Office, and was gridded at a 5° resolution and extended over the areas 0° to 40° S and 20° W to 70° E. This rainfall data set was grouped in two areas, and the standardised anomalies were calculated for the two groups: early (October, November, December) and late (January, February, March) summer seasons. These data sets were then correlated with one another. The data sets spanned the years 1949 to 1984.

In figure 3.5, from Walker (1990) an example of the simultaneous correlations between late summer and SST has been shown. Walker (1990) noted that the SOI is significantly related to Southern African rainfall. The correlation calculations were then recomputed by excluding those years when the SOI was either high of low. This meant 10 of the 36 years of the data were excluded. The new results where plotted, see figure 3.6, and showed that there was a general increase in the correlation values, and more so in the adjacent ocean basins. However, it should be noted that

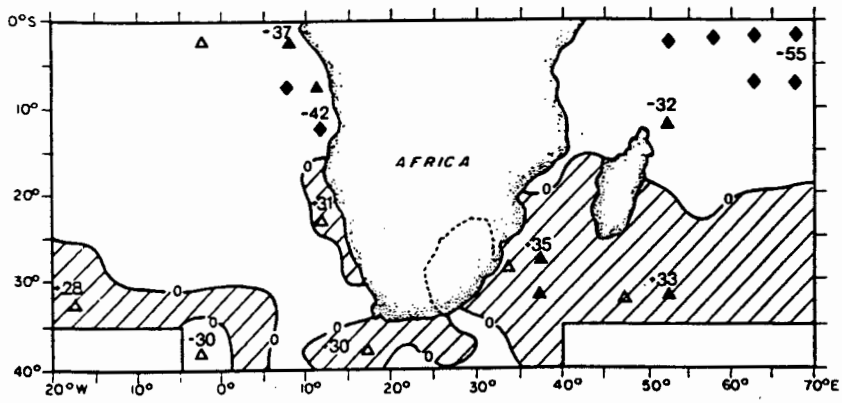

Figure 3.5: Simultaneous correlations (x 100) between area-averaged rainfall in region A and grid-square (5 ° x 5 °) SST departures in late summer (January, February, March) N=36. Significance: • 99 %; shaded ▲ 95 %; △ 90 %. From Walker, 1990.

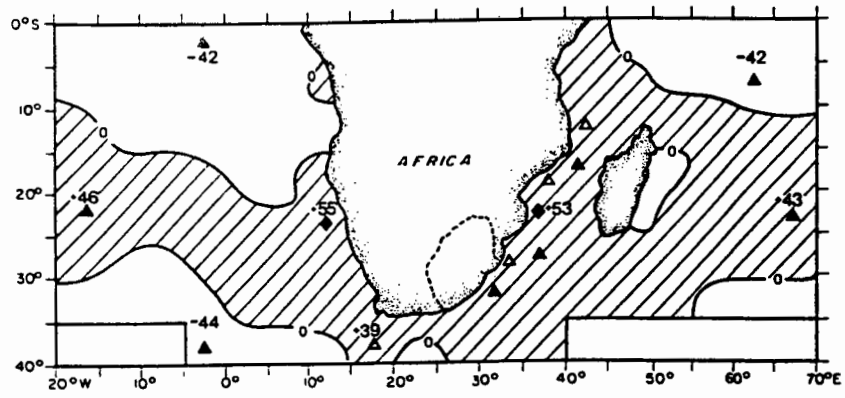

Figure 3.6: Simultaneous correlations (x 100) between area-averaged rainfall in region A and grid-square (5 ° x 5 °) SST departures in late summer (January, February, March). Southern Oscillation influence on rainfall excluded N=26. Significance: • 99 %; shaded ▲ 95 %; △ 90 %.. From Walker 1989.

there is a drop in the number of data points, and hence the number of degrees of freedom, which caused the statistical significance to change, but because of the increase in the correlation value, the statistical significance has remained

largely unchanged.

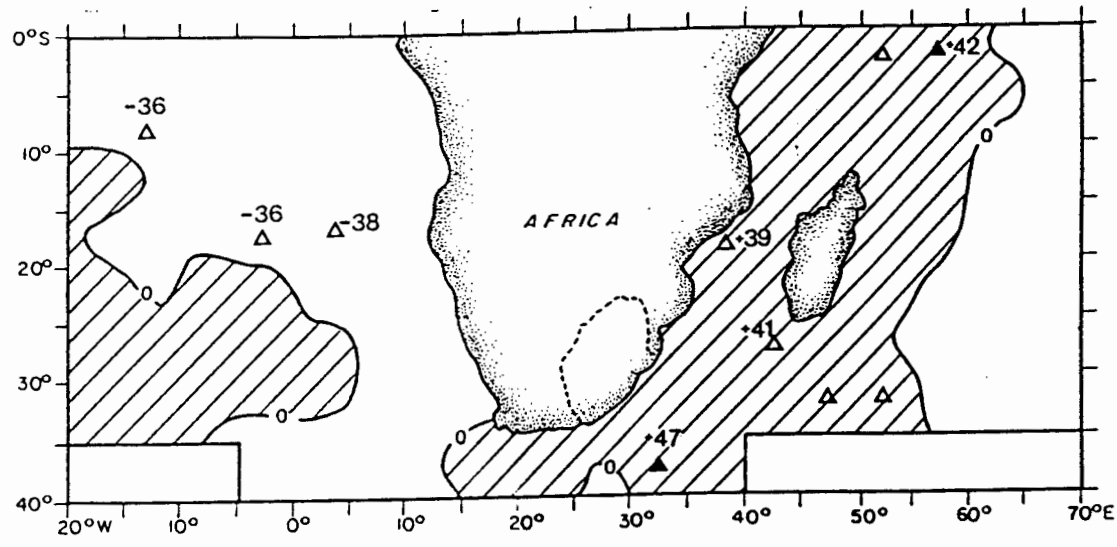

Figure 3.7: Lagged correlations (x 100) between area-averaged rainfall in region A in late summer (January, February, March) and grid-square (5 ° x 5 °) SST departures in early summer (October, November, December) Southern Oscillation influences on rainfall excluded. N=22. Significance ◇ 99 %; △ 95 %; △ 90 %. From Walker, 1989

Calculations with SST-rainfall relationships lagging by one season were computed (figure 3.7). It was shown that early summer SST variations within the Agulhas / Mozambique Current account for 15 to 25 percent of the late summer rainfall variance in the absence of the Southern Oscillations influence on these periods of rainfall. These results indicate of SST is a useful indicator of late summer rainfall. This pattern tends to be less coherent and have greater spatial variability as we look at greater resolution in both time and space scales. When the same calculations were carried out using monthly scale data these patterns changed, none the less, this work provided a starting point and a basis for further research to investigate possible dynamical links between SST and rainfall.

According to Pathack, Jury, Shillington, and Courtney (1993) low level easterly wind anomalies across the tropical south-west Indian Ocean and source regions of the Agulhas Current were found to accompany and precede the local oceanic 'warm events'. These in turn were simultaneously positively correlated with wetter conditions across the summer rainfall areas of South Africa. The implication was that the easterly wind forcing over the warmer than normal sea surface should produce enhanced moisture flux, low-level convergence and convection over the subcontinent. To the south of this region, positive SST anomalies generate greater surface heat flux anomalies and thereby increase the instability of the atmosphere and the amount of moisture within the boundary layer. At the same time, the horizontal

heat flux gradients are strengthened across the Agulhas / Subtropical Convergence front and the Agulhas Retroflection zone. The optimisation of the conditions necessary for subtropical cyclogenesis and westerly wave amplification also occurs (Jury and Walker 1988, Mey et al. 1990). Positive SST anomalies in conjunction with the intensification of tropical and temperate weather systems are believed to increase the likelihood of the formation of tropical-temperate troughs which, according to Harrison (1984), account for the majority of the rainfall in the summer rainfall area of South.

According to Walker the components of these thermodynamic mechanisms, as suggested above, have been shown to be true in other studies. Researchers Sanders and Gyakum (1980), Höflich (1984), James and Anderson (1984), Reed and Albright (1986), and Nuss and Anthes (1987) (as referenced in Walker (1989) have examined these thermodynamic mechanisms. When we look at the usefulness of the correlation with respect to rainfall prediction we note that adjacent oceanic regions do not have statistically strong lagged correlations with rainfall, however, there does seem to be consistent statistically significant lagged correlations between equatorial regions and rainfall. Therefore it can be speculated that these SSTs can be useful in empirical prediction models. Since near surface water advection is relatively strong in regions, increasing poleward from the tropics, SSTs at higher latitudes are generally not as persistent as across equatorial areas. (Pathack 1993). But SSTs at higher latitudes also show statistically significant correlation with rainfall and other meteorological variables at certain times and places (Namias 1973; Yarnal 1985; Yarnal and Kiladis 1985; Cane 1986).

Chapter 4

Data And Derived Parameters

This chapter is devoted to the examination of the data used. Main data sources were from South African rainfall measurements and the COADS data set over the adjacent oceans. Methods for deriving required parameters from the data are also discussed.

4.1 South African Rainfall

The rainfall data used in this study were obtained from the Computing Centre for Water Research (CCWR) which is located in Pietermaritzburg, South Africa. This data base includes data from thousands of rainfall stations scattered throughout South Africa. The original data set was compiled by the Department of Agricultural Engineering, University of Natal, from data collected from the following sources:

- South African Weather Bureau.
- Department of Agriculture and Water Supply.
- South African Forestry Research Institute, Department of Environment Affairs.
- South African Sugar Association Experiment Station.

- Provincial Parks Boards, organised agriculture.
- Municipalities and mines, and private individuals.

Rainfall data was then downloaded from CCWR and underwent various subjective screening procedures in order to establish a good representative sample for the regions under discussion. This screening was based on spatial and temporal homogeneity as well as the duration and quality of the time series. Data was needed for the period 1950 to 1986 as this matched the period for which SST data was available. Assuming that nearby stations experience precipitation from similar processes, monthly long-term averages were produced for each series. These series were cross-correlated, and the correlation matrix was then evaluated to find stations which correlated positively with one another.

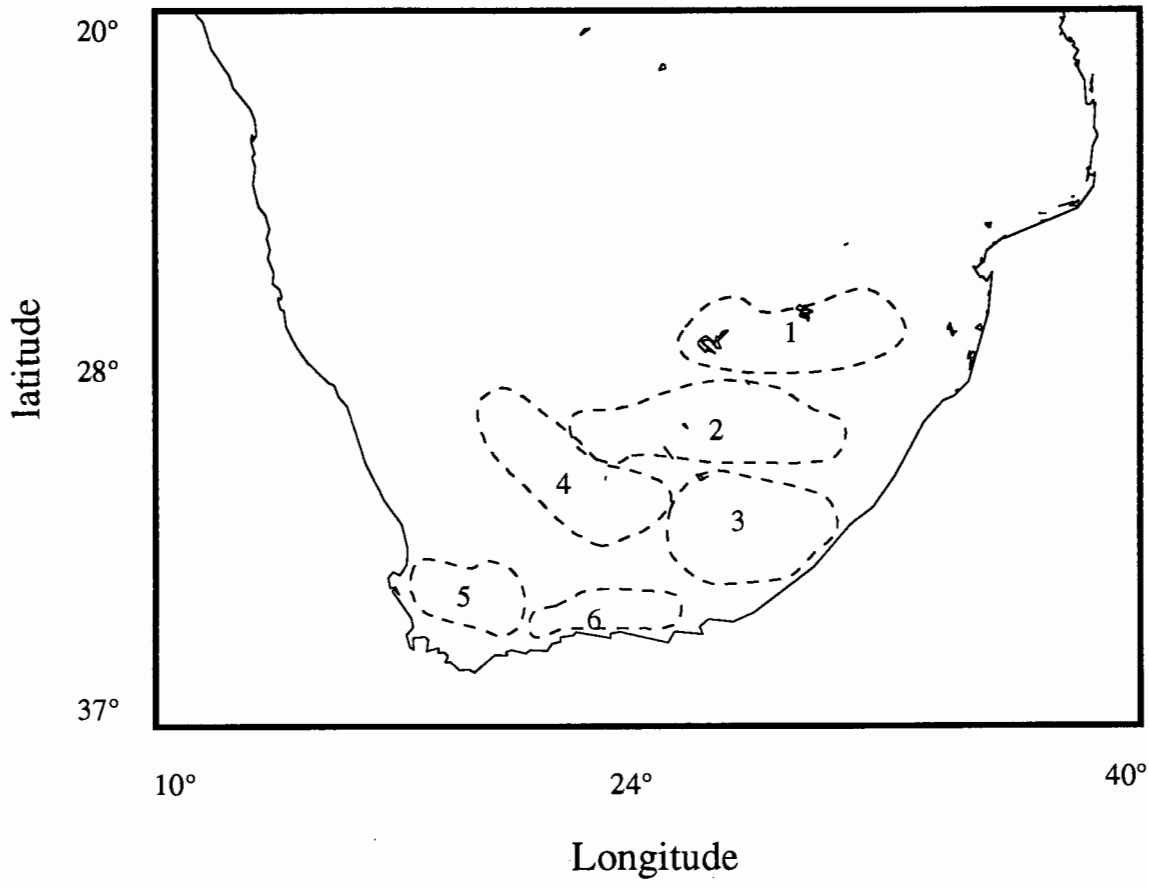

Figure 4.1: The six homogenous rainfall zones

From this analysis six homogenous rainfall zones were apparent (see figure 4.1) four of these zones are in the north-eastern parts of the country (summer rainfall region), one in the south-western Cape Province (a winter rainfall region) and one along the southern coastal and near-coastal regions of the Cape Province (which have rainfall throughout the year). A few stations did not fit into any of these six zones and were rejected on the basis that they did not have any major contribution to the rainfall distribution in that particular area. Each of the selected series was also subjectively checked for any gross errors. From the initial 1000 or so stations only 77 met the criteria and were selected. For each of these six zones a new monthly index was then calculated. Stations within each zone correlated with each other at greater than the 95 % level of confidence.

A further two zones were calculated: these comprised of zones 1 to 3 combined as zone 7 and zones 1 to 4 combined as zone 8. The stations comprising the different zones 1 to 6 are outlined in tables 4.1 to 4.6 which are located at the end of this chapter.

Figure 4.2 shows the long term area average monthly rainfall totals for the six zones. Zones 1 through 4 show similar patterns when compared to zones 5 and 6.

It should be noted that rainfall station data is notoriously "noisy" so a simple arithmetic mean of total precipitation from several stations does not necessarily produce a representative sample for an area. One technique of combining data from diverse stations is to standardise the data first (see section A.1). This technique has been used by a number of researchers, for example Kraus (1977); Nicholson (1980) and Walker (1989). This method was followed to develop the rainfall indices in each of the six different zones used in this study.

Since the main objective of this study is summer rainfall, zones 1 to 4 were considered as most important, and zones 5 & 6 were presented for completeness only. Two "all area" indices were calculated, zone 7 which includes zones 1 to 3 and zone 8 which includes zones 1 to 4.

The zones that have been formed spatially in this dissertation are similar to those in other studies, notably Nicholson 1986, Lindesay (1988b) and Walker (1989), although the method used in this study was not the same as previously used. (Note that in Walker 1990 area 1 corresponds to zone 7 in this study.)

It should be noted that statistical analysis relies on the degree of normality of the population from whence the samples originate. Although sample variables like temperature and pressure can usually be assumed to be drawn

from a normal distribution, rainfall data may follow Gamma distributions (Panofsky and Brier, 1968). In this case the data needs to be transformed to a normal distribution. However, it should be noted that satisfaction of the condition leading to normality does not guarantee normality of the series in question. It can be supposed that a particular distribution deviates from normal. January rainfall series generally show significant deviation from a Gaussian distribution, whereas the series for other months show a fairly normal distribution. An alternative to using parametric tests is to use non-parametric tests, such as the Spearman rank correlation, in contrast to the Pearson product moment correlation coefficient.

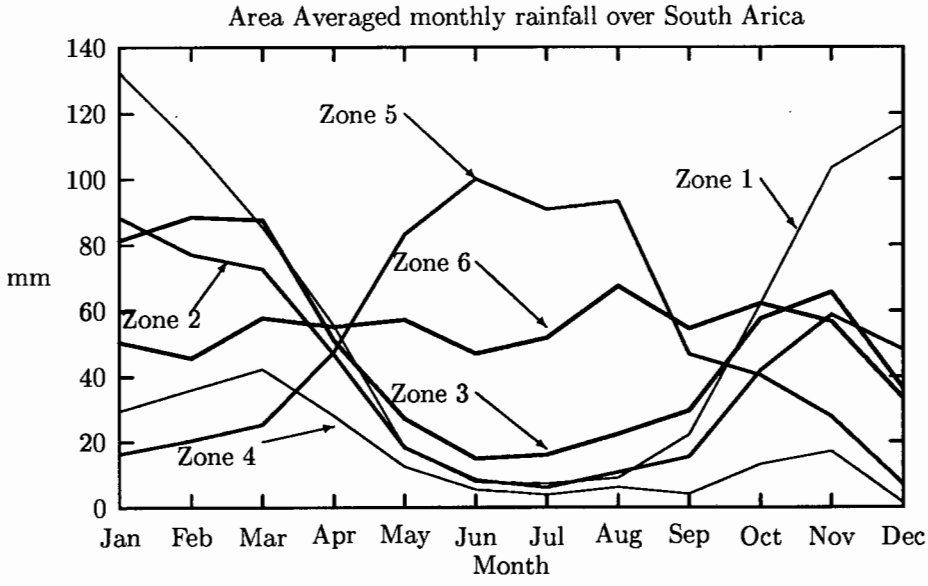

Figure 4.2: Area averaged monthly rainfall of the six zones

4.2 The Comprehensive Ocean Atmosphere Data Set

The Comprehensive Ocean Atmosphere Data Set (COADS) (Woodruff, Slutz, Jenne, and Steurer 1987) is one of the most extensive compilations of sea surface data and other marine data. Over 70 percent of the earth's surface is covered by the oceans, therefore one can not hope to understand global climate change without a clear understanding of ocean weather patterns.

COADS data records cover the period 1854—1988, 1854–1979 in *release 1* and 1980—1988 for *release 2.* COADS was developed as a co-operative effort between the National Oceanic and Atmospheric Administration (NOAA)—its Environmental Research Laboratories, National Climatic Data Center (NCDC), and Cooperative Institute for Research in Environmental Sciences (CIRES)—and the National Science Foundation's National Centre for Atmospheric Research (NCAR). The COADS project was initiated in 1981 (Slutz, Lubker, Hiscox, Woodruff, Jenne, Joseph, Steurer, and Elms 1985) and is an ongoing project.

4.2.1 Compilation of the COADS data.

The COADS project's original intention was to update the NCDC's Atlas File by using the World Meteorological Organisation (WMO) Historical Sea-Surface Temperature (HSST) data from 1854 to 1961. The COADS project did not however re-process the approximately 600 TDF-11 tapes[1] used by the Atlas project, but rather accepted the modifications already made. The above data was added to the NCDC's 1970's Decade data set, buoys, surface reading of bathythermographs and Global Telecommunication Systems data sets. To improve data coverage for the earlier years, data from other, previously unused sources such as the punch cards from South African whaling ships, was included.

The largest data set *not* used in the COADS compilation was that in the UK Marine Data Bank; its 40 million reports are generally believed to duplicate reports for UK ships that already exist in the Atlas File or HSST data (Woodruff *et al.*, 1987) Another set of data that was not included in the 1854—1979 COADS data set was remotely sensed data. A full list of all included data is available in *Release 1* of COADS (Slutz, Lubker, Hiscox, Woodruff, Jenne, Joseph, Steurer, and Elms 1985).

The data was processed at NCAR using CDC 7600 and Cray 1 computers. Processing of the greater than a 100 million data records took more than 100 hours of Cray-equivalent CPU time. Not only was all this data processed, but a new method of storing the data was devised. Originally the data was stored in the TDF-11 format on computer tape. In 1981 when NCDC completed its second revision of the Atlas Files, including data from the 1970's a new method

[1]The data on these tapes was processed from cards, which "were obtained from Ships Logs, Ship Weather Reporting Forms, published Ship Observations, Automatic Observer Buoys,Teletype Reports, and on cards purchased from several foreign Meteorological Services" (NCDC, 1968) (Woodruff et al. 1987)

was developed to store the data by removing supplementary fields, this became the TDC-1127 standard. This was changed a year later when the WMO forced NCDC to accept a new standard, TDC-1129. In compiling the COADS data set errors that had occurred in the CIRES and ERL data were corrected in the upgrade from TDC-1127 to TDC-1129 format, this was the initial processing phase. For the COADS data, NCAR's expertise in large data sets led to the design of a more efficient format than the TDC-1129. This new format halved the storage volume for the data, but resulted in no loss of information. The method they used is known as packed binary.

Once all the available data was in a uniform format, all the date sets were merged and sorted. Using the experience gained from the Alast File and 1970's Decade projects NCDC designed a quality control process that was applied to each of the observations, (See Supplement K of Slutz et al. 1985) This led to the discarding of about 30 million records. Data was then trimmed into 2° boxes. A smoothed median was calculated for each 2° box using pairs of values from adjacent boxes and months. Values were only included when a symmetric pair was present; this was done so that the temporal or spatial gradients were preserved (Woodruff *et al.*, 1987). Observations that fell outside 3.5 standard deviation (σ) limits were also discarded, those which fell out side 2.8 σ and less than 3.5 σ were flagged.

A matrix of 19 variables was used, in conjunction with the 14 statistics that are provided for each 2° × 2° box. These include basic observed values, the cross products and derived values such as wind stress. The statistics include mean, the hour the observation was taken, number of observations, standard deviation and sextile information. Because of the vastness of this data base, data is made available in various groups from the Long Marine Reports with a total size of 39.5 Gbits to Decadal Summaries Untrimmed with a size under 3 Gbits.

4.2.2 Problems With The Data Set

Over that 137 years that the COADS data set data has been collected, both methods of data collection and instruments have changed. Below is a discussion of the various problems as they relate to the actual data.

Sea Surface Temperature: SST was originally measured by the bucket method. This has now been replaced by measuring the engine-cooling-water intake. According to Woodruff, a study done by Ramage (1984) has shown that the temperature is about 0.5° C higher with the water intake method. However, it is difficult to correct for this as the data does not indicate which method was used. Also biases differ significantly depending on variations in bucket and

intake construction and use.

Wind: Firstly, the "old" Beaufort scale was used to assign wind speed. Secondly the direction was recorded as a differing compass codes (either 8, 16, 32, 36, or 360 points). To convert these speeds and directions to $m.s^{-1}$ and directions, various methods and standard lookup tables were constructed.

Time of observations: Although the time of the readings are recorded, the COADS team in the trimmed data set include a number which was the fraction of readings taken in daylight to "permit some adjustments" (Woodruff *et al.*, 1987).

Ship time and location: It has been estimated that between 6 and 8 percent of real-time ships reports (which account for 46 percent of the 1970—1979 data input) are either mislocated in position, time or both. This is, in part, due to delay in processing of data and errors in transmission. Another major problem was that of spatial coverage, not all area of the worlds oceans are equally sampled in time and space. Figure 4.3 show the spatial distribution of ships in decades from 1940 to 1979.

This dissertation used the Monthly Summary Trimmed Group (MSTG) data set. From this data set (MSTG) the following groups of data were available:

Group 3 SST, air temperature, specific and relative humidity.

Group 4 Scalar and vector winds, sea level pressure.

Group 5 total cloudiness, relative humidity, WU and WV (the latter two been wind stress parameters).

All other variables that were needed to calculate latent heat flux were derived from these values. These include dew point temperature, saturated specific humidity, potential temperature and dry air density.

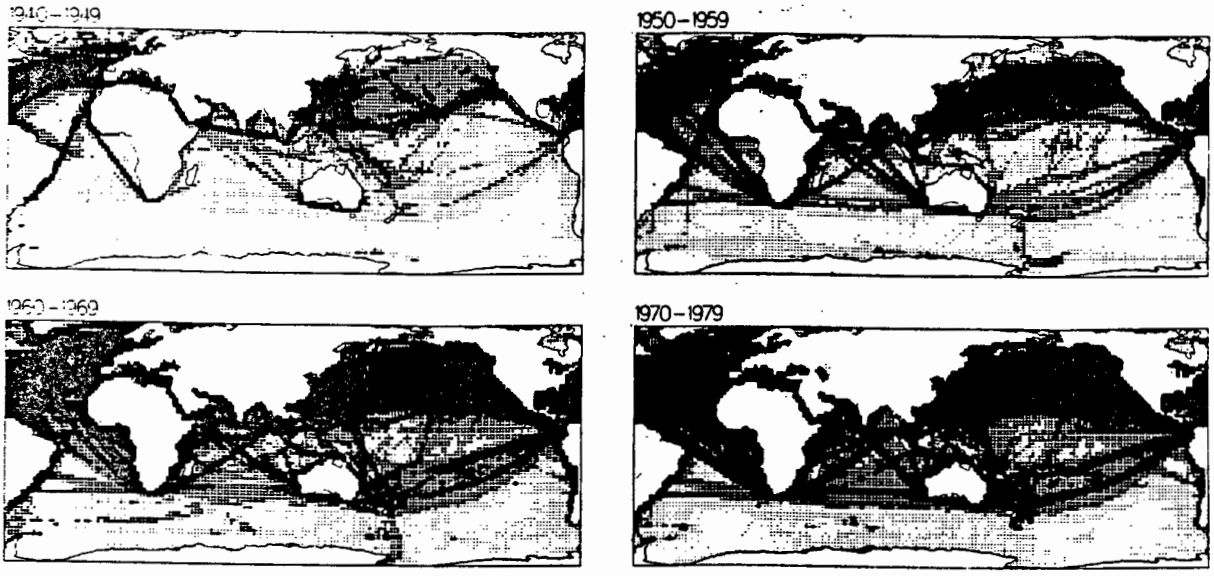

Figure 4.3: Decadal totals of SST observations (70° N — 78° S; 68° W — 68° W). The three dot sizes are from smallest at least 10, 100 or 400 observations in a 2° box per decade. From Woodruff *et al.*, 1987

4.2.3 Derivation of Other Data Variables

The region of interest chosen, was the area from 20° north to 40° south, and from 70 ° E to 120 ° E. This region was chosen because 20° north is close to the northern extend of the Indian ocean and 40° south is at the level of the Subtropical convergence.

The data from Group 3 and Group 4 were then added together so that each grid point in the region of interest had values for the SST, air temperature, specific humidity, wind speed and sea level pressure, data points that did not meet this requirement were excluded. Using this data the following parameters were derived:

- saturated specific humidity.
- potential temperature.
- air density (dry).
- scalar wind.

- latent heat of vaporization.
- sensible heat flux.
- latent heat flux.

The derivation of each of these parameters have been included below.

Saturated specific humidity Saturated specific humidity is defined as the maximum mass of water vapour that can be contained in a unit of moist air (dry air mass plus water vapour). The value was calculated from the SST and sea level pressure as follows:

First the saturated vapour pressure in millibars is calculated. Equation 4.1 is modified version of Wexler's 1976 equation for temperature less than 0° C and has an accuracy of 0.1% (Bolton 1980).

$$e_s(T) = 6.112 \times \exp\left(\frac{17.67T}{T + 243.5}\right) \tag{4.1}$$

where T (in degrees centigrade) is $-30°C \leq T \leq 35°C$.

The next step is to calculate the saturation mixing ratio(w_s). This is defined as the mass of water vapour present to the mass of dry air containing the vapour. This is given in equation 4.2 (from Hsu 1988).

$$w_s = \epsilon \frac{e_s}{p - e_s} \tag{4.2}$$

where w_s = saturation mixing ratio
ϵ = 0.62197
e_s = from equation 4.1
p = sea level pressure

Using the relationship between saturated mixing ratio (w_s) and saturated specific humidity (q_s) the latter was calculated by the following equation 4.3.

$$q_s = \frac{w_s}{1 + w_s} \tag{4.3}$$

Potential temperature Potential temperature is defined as the temperature a "parcel" of dry air would have, if reduced adiabatically to the standard pressure of 1000 hPa. It is calculated using equation 4.4

$$\Theta = T_k \left(\frac{1000}{P}\right)^{\frac{R}{C_p}} \tag{4.4}$$

where T_k = temperature in Kelvin

P = air pressure in hPa

R = gas constant for water vapour

C_p = specific heat of air at a constant pressure

Dry air density The density of dry air was derived from the equation of state for dry air. This is given in equation 4.5.

$$\rho = \frac{P}{R \times T} \tag{4.5}$$

Heat flux The calculation of heat flux has over the years been notoriously difficult and many attempts have been made to find a sound method of calculating a good approximation using bulk aerodynamic methods. Owing to the initial values that were available we will consider only latent heat flux (Q_l) and sensible heat flux (Q_s). This are defined in equations 4.17 and 4.16 respectively

Using the variables derived above the latent and sensible heat flux was calculated for each of the 2° boxes.

The atmospheric or planetary boundary layer is the frictionally dominated region between the earth's surface and the geostrophic (frictionless or synoptic) flow level. In order to understand momentum, heat and moisture transfer at the air-sea interface, study of the atmospheric surface boundary layer is very important in meteorology and physical oceanography.

The atmosphere surface boundary layer is the lowest part of the planetary boundary layer. Under conditions of horizontal homogeneity (for example over open oceans) and quasi-steady state (where time changes are so small as to be dynamically negligible) the following approximations, taken from Hsu (1988), are usually applied to the surface boundary layer:

1. The rotation of the earth, that is the Coriolis effect is unimportant in the surface boundary layer.

2. The surface boundary layer occupies the lowest 10% of the planetary boundary layer.

3. Experiments have shown that the vertical variation in stress and heat flux in the surface boundary layer is within 10% and thus the surface boundary layer is also known as the 'constant' flux layer.

4. From above it follows that in the surface boundary layer the wind direction does not change appreciably with height, thus the mean wind is described by $\overline{U}$ only.

5. The variation of mean variables with height, z, is controlled primarily by three parameters: the surface stress, the vertical heat flux at the surface and the terrain roughness.

6. Transport of atmospheric properties by turbulent diffusion (eddies) is much more important than transport by molecular diffusion.

Based on the above conditions vertical fluxes of momentum, heat and moisture in the surface boundary layer can be written:

$$\text{Wind Stress:} \quad \tau = -\rho_o \overline{u'w'} = \rho {U^2}_{\star 0}$$
$$\text{Heat Flux:} \quad H = C_p \rho_0 \overline{\theta' w'} = -C_p \rho_0 U_{\star 0} T_\star$$
$$\text{Moisture Flux:} \quad E = \rho_0 \overline{q' w'} = -\rho U_{\star 0} q_\star$$

where: u', w' are the horizontal fluctuations of the horizontal wind speed, U, and the vertical wind speed, w, respectively.

θ', q' fluctuations in potential temperature, θ, and specific humidity, q.

$-$ the means.

ρ_0 air density of reference state.

C_p specific heat at constant pressure.

$U_{\star 0}, T_\star, q_\star$ the friction (or shear) velocity of reference state, the characteristic temperature and the characteristic specific humidity respectively. (These parameters are the characteristic scales based on the Monin-Obukhov, 1954, similarity theory).

The formulas, for computing the momentum, heat and moisture fluxes, are collectively known as the eddy correlation method. The eddy correlation method is the most accurate and direct approach to estimating theses fluxes, but it is also logistically difficult for marine use (refer to section 2.2 page 23). There is another approach, the bulk methods approach, that is much easier to apply to standard data collected practically but is less accurate than the eddy correlation method (refer to section 2.2). The bulk method approach is a more practical approach and the formulae are derived as follows.

By applying scaling to the gradients (Hsu 1988, does this in detail) of the mean profiles the equations become:

$$\frac{kZ}{U_{\star 0}}(\frac{\partial \overline{U}}{\partial Z}) = \phi_m(\frac{Z}{L}) \tag{4.6}$$

$$\frac{kZ}{T_\star}(\frac{\partial \overline{\theta}}{\partial Z}) = \phi_h(\frac{Z}{L}) \tag{4.7}$$

$$\frac{kZ}{q_\star}(\frac{\partial \overline{q}}{\partial Z}) = \phi_e(\frac{Z}{L}) \tag{4.8}$$

where: k the Von Karmen constant ($\simeq 0.04$) defined such that $\phi_m(\frac{Z}{L}) = \phi_m(0) = 1$.

$m, h,$ represent momentum, heat and evaporation respectively.

L $\frac{-U^3_\star T_{vo}}{gk\theta}$ the Monin-Obukhov stability length.

T_{vo} the virtual temperature of reference state.

θ'_v the turbulent fluctuation of virtual temperature.

T'_v the virtual perturbation temperature $= T_v - T_{vo}$

T_v virtual temperature.

In order to determine the bulk methods equations each of the above equations was considered in turn. The first equation, 4.6, can be written:

$$\frac{kZ}{U_\star}(\frac{\partial U}{\partial Z}) = \phi_m(\frac{Z}{L}) \tag{4.9}$$

where: $U_\star$ replaces $U_{\star o}$ for simplicity.

Then integrating from the ground, where $Z = Z_0$ and $U = 0$, to an arbitrary height Z, one gets:

$$U_z = \frac{U_\star}{k}[ln(\frac{Z}{Z_0}) - \psi_m(\frac{Z}{L})] \tag{4.10}$$

where: $\psi_m(\frac{Z}{L}) = \int_{\frac{Z_0}{L}=0}^{\frac{Z}{L}}[1-\phi_m(\zeta)]\frac{\partial\zeta}{\zeta}$, since $\frac{Z_0}{L}$ is small in practice.

and $\zeta = \frac{Z}{L}$

The difference between level 1 (the lower elevation) and level 2 (the upper elevation) is:

$$U_2 - U_1 = \frac{U_*}{k}[ln(\frac{Z}{Z_0}) + \psi(\zeta_1) - \psi(\zeta_2)] \tag{4.11}$$

$$\Rightarrow U_\star = \frac{k(U_2 - U_1)}{[ln(\frac{Z_2}{Z_1}) + \psi_m(\frac{Z}{L})]} \tag{4.12}$$

where: $\psi_m(\frac{Z}{L}) = \psi(\zeta_1) - \psi(\zeta_2)$

$U_\star$ = shear friction velocity.

Similarly the second equation (4.7) leads to:

$$\theta_\star = \frac{k(\theta - \theta_0)}{[ln(\frac{Z_2}{Z_1}) - \psi_h(\frac{Z}{L})]} \tag{4.13}$$

and the third equation (4.8) leads to:

$$q_\star = \frac{k(q - q_0)}{[ln(\frac{Z_2}{Z_1}) + \psi_q(\frac{Z}{L})]} \tag{4.14}$$

Using these results (setting $Z_1 = Z_0$ and $Z_2 = 10\ m$) the vertical flux equations give:

$$\frac{\tau}{\rho} = U_\star^2 = \frac{k^2U_{10}^2}{[ln(\frac{10}{Z_0}) + \psi_m(\frac{10}{L})^2]} = C_0U_{10}^2 \tag{4.15}$$

$$\frac{H}{\rho C_p} = -U_\star\theta_\star = \frac{k^2U_{10}(\theta_0 - \theta_{10})}{ln(\frac{10}{z_0}) + \psi_m(\frac{10}{L})][ln(\frac{10}{Z_T}) + \psi_H(\frac{10}{L})]} = C_HU_{10}(\theta_0 - \theta_{10}) \tag{4.16}$$

$$\frac{E}{\rho} = -U_\star q_\star = C_EU_{10}(Q_0 - Q_{10}) \tag{4.17}$$

where: C_0, C_H, C_E are the transfer coefficients for the corresponding fluxes.

These equations represent the bulk aerodynamic methods for estimating the momentum, heat and moisture fluxes at the air-sea or air-land interfaces. The full set of equations has been presented here for completeness, however for this thesis only the q_s fluxes were used.

WBNO	Latitude	Longitude	Alt(m)	Station Name
508649	-25.489	25.506	1408	Slurry
509283	-25.430	26.093	1345	Doornhoek
511084	-25.544	27.027	1585	Derby
513227	-25.478	28.083	1478	Petoria-Voortrekerhoogte
515826	-25.460	29.280	1448	Middelburg
517430	-25.400	30.150	1536	Machadodorp
585056	-24.552	26.016	1158	Grootpoort
588230	-24.502	27.383	1548	Sterkfontein
591125	-24.354	29.048	969	Besonderheid "Byzonderhd"
593126	-24.360	30.049	975	Maandagshoek
595110	-24.501	31.042	880	Bosbokrand
672748	-23.586	26.551	856	Cumberland
679019	-23.489	30.011	1300	De Hoek

Table 4.1: The 13 rainfall stations in zone 1

WBNO	Latitude	Longitude	Altitude (m)	Station Name
290032	-28.323	24.316	1105	Barkly West
291148	-28.574	25.050	1161	Perdeberg
291899	-28.597	25.294	1215	Katdoornput
293007	-28.373	26.014	1306	Middelkop
295001	-28.310	27.010	1433	Winburg
299008	-28.396	29.020	1280	Clifford Chambers
356285	-27.425	22.416	1190	Hopkins
358268	-27.589	23.363	1600	Smouspoort "Mt. Carmel"
359304	-27.340	24.110	1400	Reivilo
361354	-27.541	25.116	1202	Stowlands
363571	-27.313	26.209	1295	Hendrik Theron
365444	-27.537	27.155	1430	Swartkoppie
369117	-27.576	29.036	1775	Heritage
431820	-26.412	24.282	1295	Lourensgeluk
433115	-26.552	25.042	1275	Klipfontein "Rietpan"
434888	-26.487	26.000	1475	Ottosdal
437100	-26.402	27.060	1355	Potchefstroom

Table 4.2: The 17 rainfall stations in zone 2

WBNO	Latitude	Longitude	Altitude (m)	Station Name
77522	-32.420	26.180	599	Adelaide
79215	-32.344	27.080	969	Cata
120010	-31.405	25.010	1307	Philadelphia
121875	-31.354	26.005	1318	Spitskop
125047	-31.470	27.320	1300	Nququ
126082	-31.523	28.026	1103	Nkobongo
128032	-31.320	29.028	823	Libode
172163	-30.430	25.058	1372	Colesberg
174093	-30.336	26.047	1294	Clifton
176015	-30.454	27.009	1497	Paardefontein
178881	-30.415	28.303	1364	Mnt Fletcher
180030	-31.000	29.010	1154	Papane
229737	-29.473	25.255	1387	Jagersfontein
231279	-29.392	26.100	1414	Reddersburg
232898	-29.580	27.003	1509	Quilimane

Table 4.3: The 15 rainfall stations in zone 3

WBNO	Latitude	Longitude	Altitude (m)	Station Name
165898	-30.583	21.596	1300	Carnavon
166238	-30.579	22.076	1241	Carnarvon
168066	-30.354	23.028	1155	sandpan
170099	-30.390	24.047	1244	Ebenezer (Weltevrede)
224208	-29.573	22.365	1100	Uitsig
225065	-29.352	23.030	991	Rooisloot
227054	-29.547	24.015	1140	Perdeput
251261	-29.208	21.092	793	Kenhardt
282166	-28.463	20.369	664	Kakamas
283098	-28.389	21.033	775	Geelkop
287041	-28.407	23.022	1265	Onder-Geluk
387240	-27.300	20.080	850	Noenieput
390514	-27.010	21.475	934	Matlapanen
423044	-26.446	20.018	792	Rietfontein

Table 4.4: The 14 rainfall stations in zone 4

WBNO	Latitude	Longitude	Altitude (m)	Station Name
2885	-34.450	20.001	12	Zoetendals Vallei
4723	-34.031	18.258	26	Tokai
6065	-34.042	19.030	564	Nieweberg
20649	-33.488	18.225	18	Robben Island
22038	-33.376	19.027	185	Vrugbaar
24197	-33.471	20.078	223	Montagu
60780	-33.013	17.565	18	Saldahna Bay
60864	-32.545	17.598	120	Vredenburg
62444	-32.545	18.455	229	Piketberg
66027	-32.572	20.305	1320	Dumure

Table 4.5: The 10 rainfall stations in zone 5

WBNO	Latitude	Longitude	Altitude (m)	Station Name
10742	-34.222	21.251	15	Stilbaai
11132	-34.122	21.355	168	Albertinia
12303	-34.035	22.113	91	Sandhoogte
17452	-34.017	24.465	140	Humansdorp
28150	-33.598	22.038	183	Kwepertuin
30090	-34.017	23.045	259	Concordia
32209	-33.594	24.072	235	Witelsbos
33680	-33.500	24.531	40	Hankey

Table 4.6: The 8 rainfall stations in zone 6

Chapter 5

Results obtained in the Eight Rainfall Zones

5.1 Summer rainfall and latent heat flux

In this chapter we report the results that were obtained from, firstly, a point-to-field correlation between the latent heat flux anomalies in a two by two degree longitude and latitude grid with the rainfall anomalies in the various zones. Secondly, and more comprehensively, we examine the correlation between the latent heat flux in the nine ocean key–boxes and the rainfall in each of the eight South African rainfall zones. No attempt is made to explain the significance of these results in terms of the objectives of this thesis. The interpretation of the results follow in Chapter 6.

5.2 Data

The rainfall data used in this study were extracted from the Computing Centre for Water Research (CCWR). Section 4.1 discussed the break down into the eight zones and the method used in defining these eight zones. The latent heat flux used for this section was derived from the Comprehensive Ocean Atmosphere Data Set (COADS) at a two by two degree resolution. Section 4.2 discusses the data set and derivation of the required variables. The time period considered in the following sections ranges from 1950 to 1986 inclusive for both sets of data.

Each of the data sets were standardised using equation A.1. The data was then correlated using both the Pearson

Correlation Coefficient and the Spearman Rank Correlation Coefficient. The equations for these two formulas are given in equation A.2 and equation A.7 respectively. The results of the correlation analysis were then tested with the Student's T–test. The equations used for these tests are given in equation A.3 and equation A.8 respectively.

5.3 Gridded field correlations

Initially, rainfall in each of the eight rainfall zones were correlated with each $2^\circ \times 2^\circ$ gridded ocean data point. This was done to test whether there was any large scale spatial coherency between the standardised latent heat and standardised rainfall. The latent heat flux was then lagged from zero to six months with respect to the rainfall. This was done to test whether there was any temporal coherency between the standardised latent heat and standardised rainfall. These analyses yielded poor results and the correlations were not significant. A large majority of the correlations fell between -0.3 and +0.3. There was also no significant spatial correlation. An example of this type of correlation is shown in Figure 5.1.

5.4 Key–box selection

In the second set of correlations, each of the eight rainfall zones were correlated with each of the nine oceanic key-boxes. The nine key–box areas used in this study are the same as those chosen by Pathack, Jury, Shillington, and Courtney (1993), although the previous study only examined relationship between SST and rainfall. These boxes were chosen by looking at over 300 tele-connectivity maps of standardised SST anomalies and rainfall. Areas that showed the most coherent and most significant persistent correlations were then grouped together. A list of the nine boxes are shown in table 5.1. It was initially hypothesized that similar areas would show up as key areas in relating latent heat flux to South African Summer rainfall.

These results were more encouraging, with correlations statistically significant at above the 90% level and 95% level. In the following tables the results of key–box areas that correlated at a greater that 90% significance level are tabulated. In all cases a positive correlation in the latent heat flux anomalies for a particular zone is related to an above average rainfall in the zones. If the relationship is negative for a particular key–box this means that a decrease in the

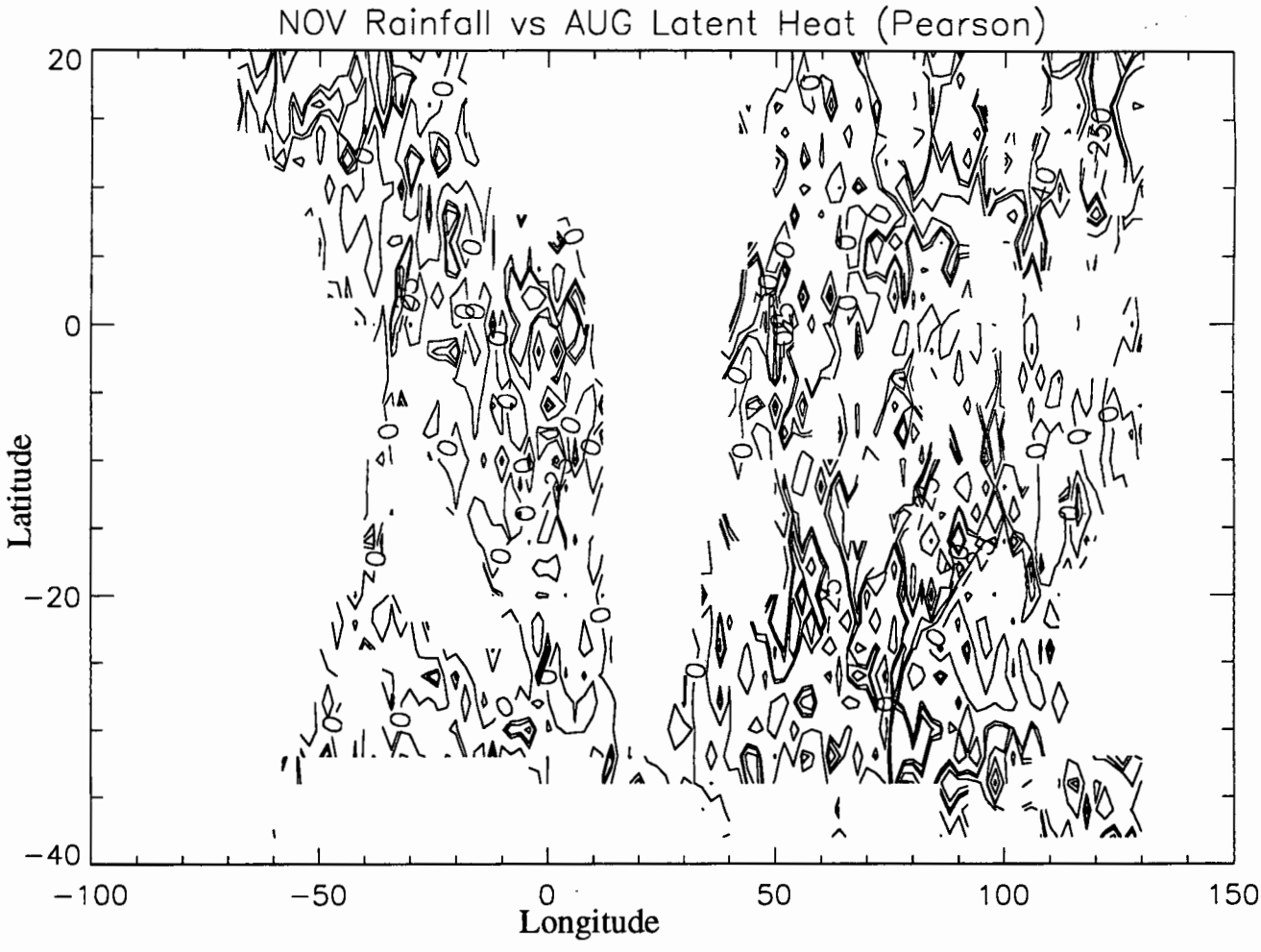

Figure 5.1: November rainfall anomalies in zone 8 correlated (Pearson) with the previous August latent heat anomalies. (R × 100)

latent heat flux anomalies leads to and increase in rainfall.

5.4.1 Zone 1 rainfall and latent heat flux

In table 5.2 correlations of rainfall anomalies in Zone 1, which is located within the Transvaal in the northeastern part of South Africa, and latent heat flux anomalies for the nine key–box areas are shown.

Abbreviation	Full name	area
CSA	Central South Atlantic	14° S–24° S, 20° W–4° E
BCR	Benguela Current Region	22° S–34° S, 10° E–16° E
ARR	Agulhas Retroflection Region	34° S–38° S, 10° E–20° E
ACR	Agulhas Current Region	28° S–36° S, 32° E–40° E
SEI	South East Indian Ocean	20° S–30° S, 80° E–100° E
WEI	Western Equatorial Indian Ocean	0° S–10° S, 40° E–60E
CEI	Central Equatorial Indian Ocean	0° S–10° S, 60° E–80° E
EEI	Eastern Equatorial Indian Ocean	0° S–10° S,80° E–100° E
ASA	Arabian Sea Area	10° S–0° N, 50° E–70° E

Table 5.1: Key boxes

Lag	October	November	December	January	February	March
0		**ACR,SEI**	ASA	**-ARR,-BCR**		-ARR,WEI
-1		ACR,-BCR	**ASA,CEI**		ACR	CEI
-2			-ASA		-ARR	
-3	-EEI		**-ASA**		**CEI**	**CEI,EEI,SEI**
-4	-CSA		**EEI**		**BCR**	**ASA,WEI**
-5		**ARR**		**-SEI**	-ACR,**-SEI**	
-6		EEI	ASA	**BCR**		SEI

Table 5.2: This table shows the correlation between the nine key box areas and Zone 1 rainfall, for the months October to March, at a greater than 90% significant level. Those key box areas with a greater than 95% significant level have been presented in bold

Above average rainfall for October was statistically linked with below average latent heat flux anomalies three months previously in the EEI region and with below average latent heat flux anomalies in the CSA region at a four month lag.

The November rainfall anomaly was directly associated with simultaneous latent heat flux anomalies in the ACR

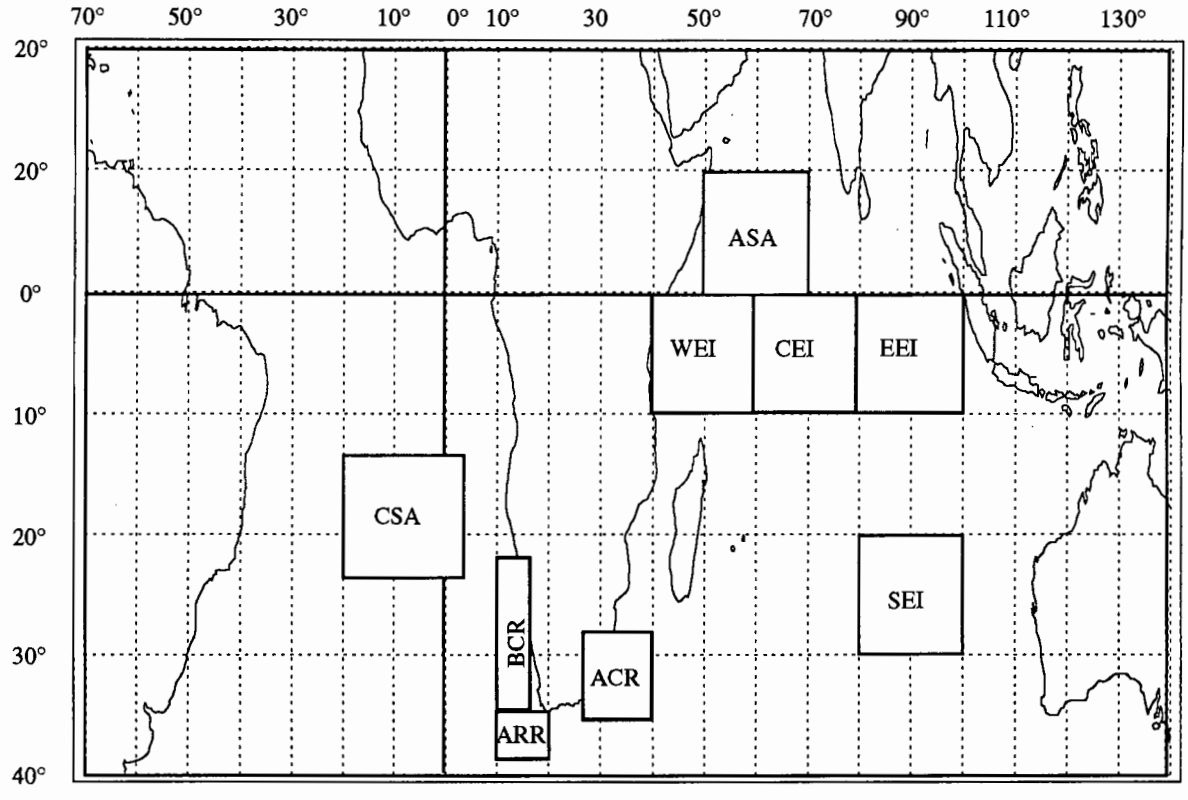

Figure 5.2: The nine regions of oceanic latent heat flux used in the study

and SEI regions. An increase in latent heat flux anomalies in the ACR region one month previously was related to an increase in rainfall; at the same time a decrease in the BCR region was noted. At a five month lag the increase of the latent heat flux anomalies in the ARR region were associated with an increase in rainfall in November. At a six month lag an increase in the latent heat flux anomalies in region EEI were associated with an increase in rainfall.

In December the rainfall anomaly were directly associated with simultaneous latent heat flux anomalies in the ASA region and a stronger association with the ASA region and the CEI region at a one month lag. The association with the ASA region is such that latent heat flux anomalies at a two and three month lag are associated with an above average rainfall. The EEI region shows an association at a four month lag. At six months the ASA region shows an association with December rainfall anomaly.

The January rainfall anomaly was directly associated with latent heat flux anomalies of the ARR and the BCR

regions. A decrease in the latent heat flux anomalies are linked with an increase in rainfall. Five months previously, the latent heat flux anomalies in the SEI region are similarly associated with January rainfall. At a six month lag, the latent heat flux anomalies in the BCR region are associated with the January rainfall anomaly.

In February only lag correlations show any significant relationships. An association with rainfall anomaly and latent heat flux anomalies in the ACR region occurs a one month lag. At a two month lag, the rainfall was associated with latent heat flux anomalies in the ARR region. The latent heat flux anomalies in the CEI region were associated with the rainfall anomaly at a three month lag; at four months the BCR region were associated with the rainfall anomaly. At a five month lag the ACR and SEI regions are associated with the rainfall anomalies such that a decrease in the latent heat flux anomalies leads to an increase in the rainfall anomaly.

In March there was an association with the latent heat flux anomalies in the ARR region and an association with the latent heat flux anomalies in the WEI region. At a one month lag the latent heat flux anomalies in the CEI region shows an association with the March rainfall anomaly. At a three month lag the latent heat flux anomalies in the CEI, EEI and SEI regions are associated with the rainfall anomaly. At the four month lag the latent heat flux anomalies in the ASA and WEI regions are associated the rainfall anomaly. At a six month lag the latent heat flux anomalies in the SEI region was positively related to the rainfall anomaly.

5.4.2 Zone 2 rainfall and latent heat flux

In table 5.3 correlations of rainfall anomalies in Zone 2, which is located mainly in the Orange Free State, and latent heat flux anomalies for the nine key–box areas are shown.

In October the rainfall anomaly were associated at one month lag with the latent heat flux anomalies in the ARR region. At a three and four month lag, there was an association with the latent heat flux anomalies in the EEI and SEI regions. At a six month lag the latent heat flux anomalies in the WEI region are associated with the rainfall anomaly.

In November, as in October, the first association found was at a one month lag, with the latent heat flux anomalies in the EEI and ASA regions. At four months the latent heat flux anomalies in the EEI and SEI regions were associated with the rainfall anomaly.

In December the latent heat flux anomalies in the CEI and CSA regions are directly associated with the rainfall

Lag	October	November	December	January	February	March
0			CEI,-CSA	**-ARR,ASA,-BCR,CEI,WEI**		**WEI**
-1	ARR	**-ASA,EEI**	ASA	**-EEI**		
-2			-ASA		**-ARR**,CEI	**ACR**
-3	**-EEI**		-ASA	**-ASA**,EEI		**CEI,EEI,SEI**
-4	**-SEI**	**EEI,SEI**	EEI		-ACR	**WEI**
-5				**-CSA,-SEI**	**-ACR**,-SEI	
-6	-WEI		WEI			

Table 5.3: As in Table 5.2, but for Zone 2

anomaly. At one, two and three months lag, the latent heat flux anomalies in the ASA region were associated with the rainfall anomaly. At four month lag the latent heat flux anomalies in the EEI region, and at a six month lag the latent heat flux anomalies in the WEI region were associated with the December rainfall anomaly.

In January there are five latent heat flux anomaly regions that show a direct association with the rainfall anomaly: these are the ARR, ASA, BCR, CEI and WEI regions. At a one month lag the latent heat flux anomalies in the EEI region shows an association with the rainfall anomaly. At a three month lag the latent heat flux anomalies in the ASA and EEI regions are associated with the rainfall anomaly. At a five month lag both the latent heat flux anomalies in the CSA region and the latent heat flux anomalies in the SEI region are associated with the rainfall anomaly.

In February, at a two month lag, the latent heat flux anomalies in the ARR and CEI regions are associated with the rainfall anomaly. At a four month lag the latent heat flux anomalies in the ACR region are associated and at five months the latent heat flux anomalies in the SEI and ACR regions show an association with the rainfall anomaly.

In March there was a direct association with the latent heat flux anomalies in the WEI region. At a two month lag the latent heat flux anomalies in the ACR region are associated with the rainfall anomaly. The latent heat flux anomalies in the CEI, EEI SEI regions are associated, with the rainfall anomaly. At a four month lag the WEI region was associated with the rainfall anomaly.

5.4.3 Zone 3 rainfall and latent heat flux

In table 5.4 correlations of rainfall anomalies in Zone 3, which is located in the northeastern regions of the Cape Province and covers areas to the south and west of Lesotho, and latent heat flux anomalies for the nine key–box areas are shown.

Lag	October	November	December	January	February	March
0	**-WEI**		**-CSA**	**ASA,-BCR**		**WEI**
-1	ARR,-EEI	**-ASA**,CSA	**-SEI**	**-EEI**	-ARR,-CSA	ACR
-2			**-ASA,-SEI**		-ARR,-BCR	-CSA
-3		-ACR,-WEI	**-ACR,-ASA**,-CEI	-ACR,-ASA,**-SEI**,-WEI		EEI,SEI
-4		SEI	**-ASA**,EEI			
-5	**-BCR**,-CSA	-ACR,CSA		**CEI,-SEI**	**-ACR**	
-6	-CSA,-WEI			**-ACR,-CSA**		-ARR

Table 5.4: As in Table 5.2, but for Zone 3

In October the latent heat flux anomalies in the WEI region was directly associated with the rainfall anomaly in Zone 3. At a one month lag the latent heat flux anomalies in the ARR and EEI regions are associated with the rainfall anomaly. The latent heat flux anomalies in the regions BCR and CSA from five months previously are associated with the October rainfall anomaly. At a six month lag the latent heat flux anomalies in the regions CSA and WEI are also associated with the rainfall anomaly.

In November there was an association at a one month lag with the latent heat flux anomalies for the regions ASA and CSA and the rainfall anomaly. At a three month lag there was an association with the latent heat flux anomalies in the regions ACR and WEI. Four months previously there was an association with the latent heat flux anomalies in the SEI region. At a five month lag the latent heat flux anomalies in the ACR and CSA regions are associated with the rainfall anomaly.

In December the zero, one, two and three months lags all show negative correlation with a greater than 95 % significance with the exception of the CEI region at a three month lag. For the zero lag the latent heat flux anomalies in the CSA region, at the one month lag the latent heat flux anomalies in the SEI region, at the two month lag the latent

heat flux anomalies in the ASA and the latent heat flux anomalies in the SEI regions, and at the three month lag the latent heat flux anomalies in the ACR, in the ASA, and CEI regions are all associated with the rainfall anomaly. At the four month lag the latent heat flux anomalies of the EEI and ASA regions are associated with the rainfall anomaly.

In January at zero lag the latent heat flux anomalies in the ASA and BCR regions are associated with the rainfall anomaly. At a one month lag the latent heat flux anomalies in the EEI region was associated with the rainfall anomaly. At a three month lag all four regions, ACR, ASA, SEI and WEI are associated with the rainfall anomaly. For a five month lag the latent heat flux anomalies in the region CEI and SEI are associated with the rainfall anomaly. Lastly, the regions ACR and CSA region are associated with the rainfall anomaly at a six month lag.

At one month lag the latent heat flux anomalies in the ARR and CSA regions are associated with the rainfall anomaly for the month of February. At a two month lag the latent heat flux anomalies in the ARR and BCR regions show an association with the rainfall anomaly. Lastly at a five month lag the ACR regions latent heat flux anomalies are associated with the rainfall anomaly in Zone 3.

The latent heat flux anomalies in the WEI region are directly associated with the rainfall anomaly for the month of March. At one month lag the latent heat flux anomalies in the ACR region shows an association with the rainfall anomaly. At a two months lag the latent heat flux anomalies in the CSA region shows an association with the rainfall anomaly. At a three month lag the latent heat flux anomalies in the regions EEI and SEI show an association with the rainfall anomaly and at six months ARR latent heat flux anomalies shows an association with the March rainfall anomaly.

5.4.4 Zone 4 rainfall and latent heat flux

In table 5.5 correlations of rainfall anomalies in Zone 4, which is located in the northern regions of the Cape Province and parts of the Greater Karoo (which is a dry area), and latent heat flux anomalies for the nine key–box areas are shown.

In October the first association between the latent heat flux anomalies and rainfall anomaly occurs at a one month lag, with the region EEI. The only other associations are at a four months lag. These are the with the latent heat flux anomalies in the SEI and CEI regions.

Lag	October	November	December	January	February	March
0		-WEI	-CSA	-ARR,-BCR,**WEI,**		WEI
-1	-EEI	-ASA,**EEI**	**-ARR**	**-EEI,-SEI**		ACR,CSA
-2		**-CSA**			-ARR,-**WEI**	ACR
-3				**-ASA**,EEI		ASA,CEI
-4	**CEI**,-SEI					**WEI**
-5		**-ACR**		-ASA,**EEI**,-SEI,	**-ACR**	
-6				-CSA		

Table 5.5: As in Table 5.2, but for Zone 4

In November the latent heat flux anomalies in the WEI region was directly associated with the rainfall of Zone 4. At a one month lag it was associated with the latent heat flux anomalies in the ASA and EEI regions. At a two month lag the latent heat flux anomalies in the CSA region are associated with the rainfall anomaly. At a five month lag the latent heat flux anomalies in the ACR region are associated with the rainfall anomaly.

In December at zero lag the CSA region shows a direct inverse association with the Zone 4 rainfall, at a one month lag there was a stronger inverse association with the latent heat flux anomalies in the ARR region.

In January at zero lag the latent heat flux anomalies in the ARR, WEI and BCR regions show an association with the rainfall anomaly. The rainfall anomaly was associated with the latent heat flux anomalies of the regions EEI and SEI at a one month lag. The latent heat flux anomalies of the regions EEI and ASA shows an association at the three month lag. At a five month lag the regions ASA, EEI and SEI latent heat flux anomalies show an association with the rainfall anomaly of this zone. Lastly, at a six month lag the latent heat flux anomalies of the CSA region are associated with the rainfall anomaly for the month of January.

In February the first association occurs at a two month lag with the latent heat flux anomalies of the regions ARR and WEI. At a five month lag there was an association with the latent heat flux anomalies of the ACR region and the rainfall anomaly.

In March there was a direct association with the latent heat flux anomalies of the WEI region. At a one month lag the latent heat flux anomalies of the regions ACR and CSA, and again at the two month lag the ACR region is

associated with the rainfall anomaly. At a three month the latent heat flux anomalies of the ASA and CEI regions are associated with the rainfall anomaly. The latent heat flux anomalies of the WEI region at a four month lag are associated with the rainfall anomaly for March of Zone 4.

5.4.5 Zone 5 rainfall and latent heat flux

In table 5.6 correlations of rainfall anomalies in Zone 5, which is located in the southwest extremes of South Africa and experiences mainly winter rainfall, and latent heat flux anomalies for the nine key–box areas are shown. This zone has been included for completeness.

Lag	October	November	December	January	February	March
0			**BCR**,WEI			
-1	-BCR		-WEI		ACR,BCR	**-CEI,-EEI**
-2	**CEI**,-SEI	CEI,WEI	-CSA		**BCR**	BCR
-3	-SEI	WEI			ACR,-BCR	
-4			**ACR**,SEI		-EEI	
-5	**-BCR**	-CSA	ACR,**-EEI**,-WEI,	**ARR**	**CSA**	**-BCR**,-CEI,-CSA,**EEI**
-6		**EEI**				**SEI**

Table 5.6: As in Table 5.2, but for Zone 5

In October there was an association with the latent heat flux anomalies in the BCR region at a one month lag. At a two month lag, there was an association of the latent heat flux anomalies in the CEI and SEI region with the rainfall anomaly. The association with the SEI region holds for the third month as well. In the fifth month, the latent heat flux anomalies in the BCR region shows an association with the rainfall anomaly.

In November the first associations occur at the two month lag. This was with the latent heat flux anomalies in the CEI and WEI regions. At a three month lag the latent heat flux anomalies in the WEI region are again associated with the rainfall anomaly. At a five month lag the latent heat flux anomalies in the CSA region shows an association and at a six month lag the latent heat flux anomalies in the EEI region are associated with the rainfall anomaly.

In December there was a direct association with the latent heat flux anomalies in the BCR and WEI regions. At a one month lag this association was with the latent heat flux anomalies in the WEI region and at a two month lag with the latent heat flux anomalies in the CSA region. At a four month lag there was an association with the latent heat flux anomalies in the ACR and SEI regions. At a five month lag an association was found with the latent heat flux anomalies in the ACR, EEI and WEI regions and the rainfall anomaly of the Zone 5.

In January the only one association was found between Zone 5 rainfall anomaly and the latent heat flux anomalies . This was an association with the latent heat flux anomalies in the ARR region at a five moth lag.

In February the latent heat flux anomalies in the ACR and BCR regions are associated at a one month lag. At a two month lag the latent heat flux anomalies in the BCR region is associated with the rainfall anomaly. At a three month lag the latent heat flux anomalies in the ACR and BCR regions are associated with the rainfall anomaly. At a four month lag the latent heat flux anomalies in the EEI region are associated and at a five month lag the latent heat flux anomalies in the CSA region was associated with the zones rainfall anomaly.

In March the first association between latent heat flux anomalies and the rainfall anomaly occurs at a one month lag with the CEI and EEI regions. At a two month lag, the latent heat flux anomalies in the BCR region again associated with the rainfall anomaly. At a five month lag the latent heat flux anomalies in the BCR, CEI, CSA and EEI regions were associated with the rainfall anomaly. The latent heat flux anomalies at a six months lag in the SEI region are associated with the rainfall anomaly in Zone 5.

5.4.6 Zone 6 rainfall and latent heat flux

In table 5.7 correlations of rainfall anomalies in Zone 6, which is located in the southern extremes of South Africa and experiences rainfall throughout the year, and latent heat flux anomalies for the nine key–box areas are shown. This zone has been included for completeness.

In October there was a direct association between the rainfall anomaly and the latent heat flux anomalies of the regions ACR, BCR, SEI and WEI. At a one month lag, latent heat flux anomalies in the two ARR and BCR regions were associated with rainfall anomaly. At a two month lag the latent heat flux anomalies in the EEI region were associated with the rainfall anomaly. The only other association was at a six month lag and this was with the latent

Lag	October	November	December	January	February	March
0	**-ACR**,-BCR,-SEI,-WEI	**EEI**	-CSA,-SEI	WEI		-CSA,**WEI**
-1	**ARR,BCR**	**CSA**		**-BCR**	ACR,**BCR**,**-CSA**	-CEI,**-EEI**
-2	EEI		-CEI,**-SEI**,**-WEI**			
-3			-EEI			
-4		EEI		CSA,**EEI**	**-EEI**	
-5			**-ACR**,**-EEI**,-WEI	-SEI	**CSA**	
-6	-CSA				-BCR	**SEI**

Table 5.7: As in Table 5.2, but for Zone 6

heat flux anomalies of the CSA region.

In November there was a direct association between the latent heat flux anomalies of the region EEI and the rainfall anomaly. At a one month lag the latent heat flux anomalies of the CSA region was associated with the rainfall anomaly. The only other association that occurred was with the latent heat flux anomalies in the EEI region at a four month lag.

In December the latent heat flux anomalies in the CSA and SEI regions are associated a two month lag with the rainfall anomaly. The latent heat flux anomalies with a two month lag in the CEI, SEI and WEI regions are associated with the rainfall anomaly. The latent heat flux anomalies in the EEI region are associated with the rainfall anomaly at a three month lag. Lastly the latent heat flux anomalies in the ACR, EEI and WEI regions are associated with the rainfall anomaly in the Zone 6.

In January the latent heat flux anomalies in the region WEI were directly associated with the rainfall anomaly. At a one month lag the latent heat flux anomalies in the BCR region were associated with the rainfall anomaly. At a four month lag the latent heat flux anomalies in the EEI and CSA regions were associated with the rainfall anomaly. At a five month lag the latent heat flux anomalies in the SEI region were associated with the rainfall anomaly.

In February the first association was at a one month lag, and this was with the latent heat flux anomalies in the ACR, BCR and CSA regions. At a four month lag the latent heat flux anomalies in the EEI regions are associated with the rainfall anomaly. The latent heat flux anomalies in the CSA region and the rainfall anomaly are associated

at a five month lag, and at a six month lag, the latent heat flux anomalies in the BCR region are associated with the rainfall anomaly.

In March the latent heat flux anomalies in the CSA and WEI regions were directly associated with the Zone 6 rainfall anomaly. At the one month lag the latent heat flux anomalies in the CEI and EEI regions are associated with the rainfall anomaly. The only other association with the rainfall anomaly occurs at a six month lag with the latent heat flux anomalies in the SEI region.

5.4.7 Zone 7 rainfall and latent heat flux

In table 5.8, correlations of rainfall anomalies in Zone 7, which is a combination of zones 1, 2 and 3 and represents the majority of the summer rainfall region, and latent heat flux anomalies for the nine key–box areas are shown.

Lag	October	November	December	January	February	March
0			CEI,-CSA	**-ARR,ASA**,-BCR,		**WEI**
-1	ARR	**-ASA**,EEI		**-EEI**		
-2			**-ASA**		**-ARR**	
-3	**-EEI**		-ACR,**-ASA**,-CEI	**-ASA**,EEI,-SEI,		**CEI,EEI,SEI**
-4	-SEI	EEI,SEI	**EEI**		BCR	**WEI**
-5	-BCR			-CSA,**-SEI**	**-ACR**,-SEI	
-6	-WEI			BCR		

Table 5.8: As in Table 5.2, but for Zone 7

In October the first association of Zone 7 rainfall anomaly was with the latent heat flux anomalies of the ARR region at a one month lag. At a three month lag the latent heat flux anomalies of the EEI region are associated with the rainfall anomaly. At a four month lag the latent heat flux anomalies in the SEI region are associated with the rainfall anomaly. At a five month lag the latent heat flux anomalies in the BCR region are associated with the rainfall anomaly. Lastly the latent heat flux anomalies in the WEI regions at a six months lag was associated with the rainfall anomaly.

In November the latent heat flux anomalies in the ASA and EEI regions are associated with the rainfall anomaly at a two month lag. At a four month lag the latent heat flux anomalies of the EEI the SEI regions are associated with the rainfall anomaly in Zone 7.

In December the CEI and CSA regions are directly associated with the rainfall anomaly. At a two month lag the latent heat flux anomalies in the ASA region are associated with the rainfall anomaly. At a three month lag the latent heat flux anomalies in the ACR, ASA and CEI regions are associated with the rainfall anomaly. At a four month lag the latent heat flux anomalies in the region EEI are associated with the rainfall anomaly.

In January the latent heat flux anomalies in the regions ARR, ASA and BCR are directly associated with the rainfall anomaly in this zone. At a one month lag the latent heat flux anomalies in the EEI region are associated with the rainfall anomaly. At a three month lag the latent heat flux anomalies in the regions ASA, EEI and SEI associated with the rainfall anomaly. Both the ASA and SEI region's latent heat flux anomalies associated with the rainfall anomaly at a five months lag. At a six month lag the latent heat flux anomalies in the BCR region were associated with the rainfall anomaly.

In February, at a two month lag the latent heat flux anomalies in the ARR region were associated with the rainfall anomaly. The latent heat flux anomalies in the BCR region were associated at a four month lag with the ACR and SEI regions both associated at a five month lag with the rainfall anomaly of this zone.

There was direct association between the latent heat flux anomalies in the WEI region and the March rainfall anomaly were noted. At a three month lag the CEI, EEI and SEI regions associated with this rainfall anomaly, and again at a four month lag the latent heat flux anomalies of the WEI region were associated with the rainfall anomaly.

5.4.8 Zone 8 rainfall and latent heat flux

In table 5.9 correlations of rainfall anomalies in Zone 8, which is a combination of zones 1, 2, 3 and 4 and represents the majority of the summer rainfall region, and latent heat flux anomalies for the nine key–box areas are shown.

In October the first association occurs at a one month lag with the latent heat flux anomalies in the ARR and EEI regions. At a three month lag the latent heat flux anomalies in the EEI region are associated with the rainfall anomaly. At a four month lag the latent heat flux anomalies in the SEI region were associated, as was the latent heat

Lag	October	November	December	January	February	March
0			**-CSA**	-ARR,**ASA**,**-BCR**,WEI		**WEI**
-1	ARR,-EEI	**-ASA**,EEI		**-EEI**		
-2			**-ASA**		**-ARR**	
-3	**-EEI**		-ACR,**-ASA**	**-ASA**,EEI,-SEI,		ASA,**CEI**,**EEI**,**SEI**
-4	-SEI	SEI	**EEI**			**WEI**
-5	-BCR			**-SEI**	**-ACR**	
-6	-WEI			BCR		

Table 5.9: As in Table 5.2, but for Zone 8

flux anomalies in the BCR region at five month lag and the latent heat flux anomalies in the WEI region at a six month lag with the rainfall anomaly.

In November at a one month lag the latent heat flux anomalies in the ASA and EEI regions are associated with the Zone 8 rainfall anomaly. At a four month lag the latent heat flux anomalies in the SEI region are associated with the rainfall anomaly.

In December the latent heat flux anomalies in the CSA region are associated with the rainfall anomaly. At a two month lag the latent heat flux anomalies in the ASA region was associated with the rainfall anomaly. At a three month lag the latent heat flux anomalies in the ACR and ASA region are both associated with the rainfall anomaly for the month December. At a four month lag the latent heat flux anomalies in the EEI region are associated with the rainfall anomaly of Zone 8.

In January there was a direct association between the latent heat flux anomalies of the regions ARR ASA, BCR and WEI with the rainfall anomaly. At a one month lag the latent heat flux anomalies in the EEI region are associated with the rainfall anomaly. At a three month lag the latent heat flux anomalies in the regions ASA, EEI and SEI are associated once again with the rainfall anomaly. At a five month lag the latent heat flux anomalies in the SEI region is associated with the rainfall anomaly and lastly, at a six month lag the latent heat flux anomalies in the BCR region are associated with the rainfall anomaly as well.

In February the latent heat flux anomalies in the ARR region are associated at a two month lag with the rainfall

anomaly. The latent heat flux anomalies in the ACR region at a five month lag are also associated with the rainfall anomaly.

In March the latent heat flux anomalies in the WEI region were directly associated with the rainfall anomaly for the Zone 8. At a three month lag the latent heat flux anomalies in the following regions were associated with the rainfall anomaly: ASA, CEI, EEI and SEI. The latent heat flux anomalies in the WEI region at a four month lag were associated with the rainfall anomaly for the month of March.

Chapter 6

Discussion and Conclusions

These results are discussed in this chapter. Interpretations based on the results are related to the objectives of the dissertation. Problems encountered are addressed and a direction for future work is suggested.

Chapter 5 listed the eight South African rainfall zones that were studied. For each of these zones, a list of the most significant correlations that occurred with the oceanic latent heat flux anomalies was tabulated. These results are examined closely, focusing on the four main summer rainfall zones, labeled one, two, three and four, and the zones numbered seven and eight. The latter two are the averages of zones one, two and three and one to four respectively. Rather than looking exclusively at the particular rainfall zones, we examine each of the summer rainfall months (October to March) and highlight the regions of oceanic latent heat flux anomalies that correlate directly or are lag correlated with these regions. This approach shows which of these latent heat flux regions is most significant in the summer rainfall distribution.

6.1 Background to the Experiment

Figure 5.2 shows the nine regions of oceanic latent heat flux and their relative areas and spatial distribution. These regions were chosen on the basis of the previous study of Pathack, Jury, Shillington, and Courtney (1993). The procedure for their selection has been outlined in section 5.4.

The six rainfall zones, (eight if the two combined areas are considered) are shown schematically in figure 6.1. These zones were chosen on the basis of those zones used in the study by Pathack, Jury, Shillington, and Courtney (1993) and their selection criteria has been outlined in section 4.1.

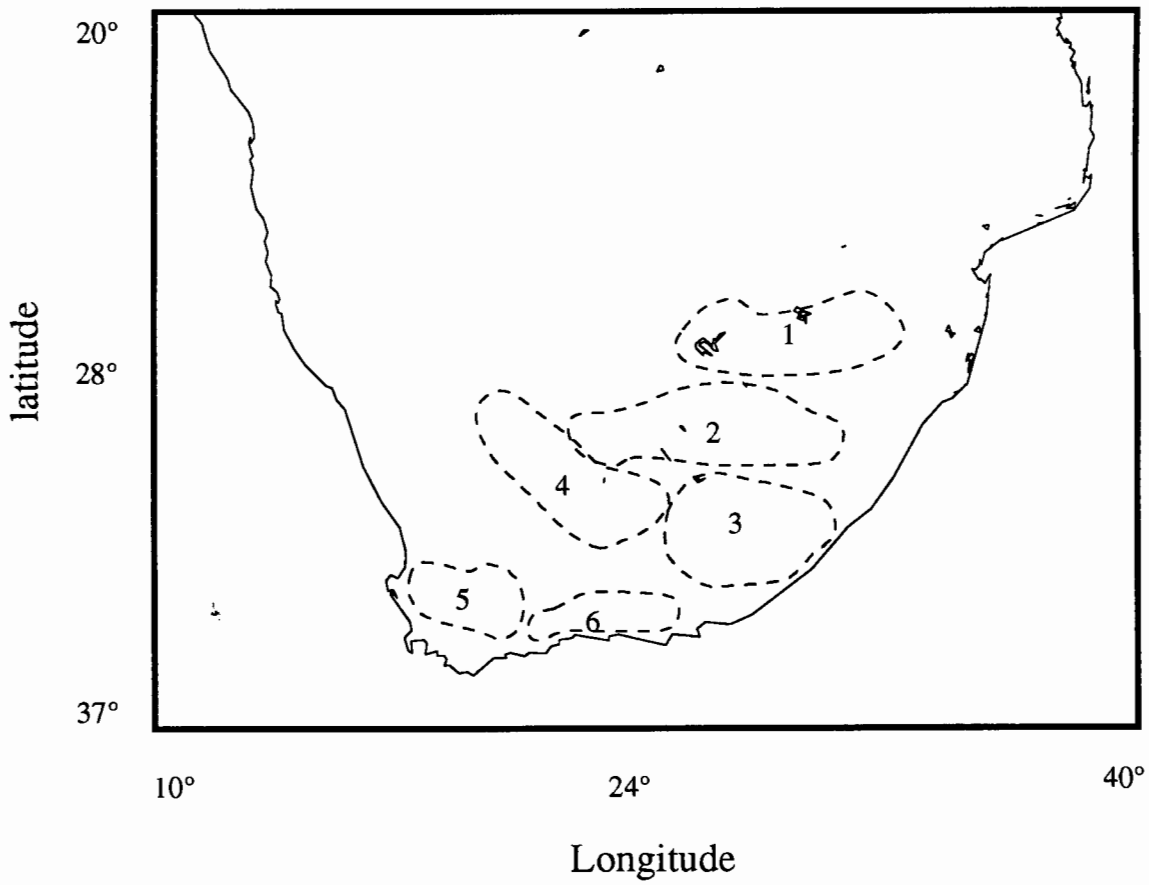

Figure 6.1: The six zones of rainfall used in the study

Using the rainfall data from these zones and the oceanic latent heat flux from the nine regions, the anomalies of rainfall and oceanic latent heat flux were correlated with the latent heat flux anomalies lagging the rainfall anomalies by up to six months. A summary of the most significant results are presented below:

6.2 Summary of results

In this section rather than looking at each of the rainfall zones and the correlation of the various regions of oceanic latent heat flux anomalies with each of the zones individually, we examine the four summer rainfall zones and the two areal averages for each of the summer rainfall months (October to March) in order the establish a relationship, if any, of oceanic latent heat flux anomalies with a particular rainfall month. To achieve this a table was constructed which lists all the latent heat flux regions in the six rainfall zones that showed some form of persistence across all zones. This persistence could be the same oceanic region correlating at the same lag in at least three of the rainfall zones or if a oceanic region showed some form of persistent correlation at varying lags. The idea was to find a general pattern or group of patterns for each rainfall month thereby identifying which oceanic regions are significant from a precursor or predictor point of view. The values are listed in the table in the following format: "SRRR-L" where "S" is the sign of the correlation, this is left blank for a positive correlation; "RRR" is the name of the region and "L" is the lag in months at which the correlation occurred. For example "-ARR-3" would indicate a negative correlation with the region ARR (Agulhas Retroflection Region) at a three month lag.

For each of the six summer rainfall months, October to March, a table of the regions of latent heat flux anomalies that correlated, using the criteria outlined above, is shown below:

October results

Zone	Regions		
1		-EEI-3	
2		-EEI-3	ARR-1
3	-EEI-1		ARR-1
4	-EEI-1		
7		-EEI-3	ARR-1
8	-EEI-1	-EEI-3	ARR-1

Table 6.1: October results

In October the area correlation that is most significant in all the rainfall zones considered, is the oceanic region EEI. This shows that a negative correlation with a one month lag in the latent heat flux anomaly, is present with the rainfall zones 3, 4 and 8. The other zones; 1, 2, 7 and again 8 show a negative correlation with the region EEI at a three month lag in the latent heat flux anomaly. The region ARR also has significant positive correlations with the regions 2, 3, 7 and 8. Therefore in all cases a below average latent heat flux anomalies in the EEI or ARR region is associated with above average rainfall. These results could be linked to Summer Monsoon. The Summer Monsoon is marked by a strong southwest wind in the northern hemisphere which is a continuation of the southern hemispheres Trades (Tomczak and Godfrey 1994). The EEI region correlates with the October rainfall at a one and three month lag, that is the July and September EEI region's latent heat flux are associated with the rainfall. This is noted because these months fall either side of the peak in Summer Monsoon. This may indicate the variability of the Monsoon has direct bearing on the October rainfall anomaly as the South Indian Anticyclone is at is furtherest north during this month and this is one of the rain bearing system for these zones.

November results

Zone	Region
1	
2	-ASA-1
3	-ASA-1
4	-ASA-1
7	-ASA-1
8	-ASA-1

Table 6.2: November results

With the exception of the rainfall zone 1 the region ASA correlated negatively with a one month lag with all the rainfall zones. Thus a decrease in the latent heat flux is associated with an increase in the rainfall. November is the month of transition from the Summer Monsoon to the Winter Monsoon over the ASA area. The winds at this time of year turn easterly at the equator.

December results

Zone	Regions		
1	-ASA-2	-ASA-3	EEI-4
2	-ASA-2	-ASA-3	EEI-4
3	-ASA-2	-ASA-3	EEI-4
4			
7	-ASA-2	-ASA-3	EEI-4
8	-ASA-2	-ASA-3	EEI-4

Table 6.3: December results

In December all the correlations with the ASA region were negative. All rainfall zones with the exception of zone 4 correlate significantly with one of the oceanic latent heat flux anomaly region. Zones 1 to 3, 7 and 8 correlate with the ASA region at a two and three month lag with the latent heat flux anomalies. These rainfall zones also correlate with the EEI region at a four month lag.

The winds over these areas are now northeasterly in December. At lag the wind over the areas are southwesterly and the peak Summer Monsoon occurs at a four month lag, which is the same time the EEI region correlates. Thus a decrease in the latent heat flux anomalies at these times is associated with and increase in the rainfall.

January results

Zone	Regions	
1	-ARR-0	-BCR-0
2	-ARR-0	-BCR-0
3		-BCR-0
4	-ARR-0	-BCR-0
7	-ARR-0	-BCR-0
8	-ARR-0	-BCR-0

Table 6.4: January results

In January the pattern changes from the previous months with all correlations being negatively correlated with the two oceanic regions surrounding the country, ARR and BCR. With the exception of the rainfall zone 3, with which only the BCR correlates, they all correlate negatively at zero lag. In this month the tele-connections with remote regions seem to be cut off. Atmospherically the ITCZ has moved southwards.

February results

Zone	Regions	
1	-ARR-2	-ACR-5
2	-ARR-2	-ACR-5
3	-ARR-2	-ACR-5
4	-ARR-2	-ACR-5
7	-ARR-2	-ACR-5
8	-ARR-2	-ACR-5

Table 6.5: February results

In February the region ARR negatively correlated with the all the rainfall zones, at a two month lag. The region ACR correlated with all rainfall zones, with a negative correlation at a five month lag. These regions are also close to the coast of southern Africa. The association is that the ARR and ACR regions lag the rainfall in all zones. It is at this time that the Northeastern Monsoon wind peaks in the northern hemisphere.

March results

Zone	Regions				
1	WEI-0	WEI-4	CEI-3	EEI-3	SEI-3
2	WEI-0	WEI-4	CEI-3	EEI-3	SEI-3
3	WEI-0			EEI-3	SEI-3
4	WEI-0	WEI-4	CEI-3		
7	WEI-0	WEI-4	CEI-3	EEI-3	SEI-3
8	WEI-0	WEI-4	CEI-3	EEI-3	SEI-3

Table 6.6: March results

In March, three Indian Ocean regions correlated positively with the rainfall zones. The first correlation tabulated is a simultaneous correlation with the WEI region. This oceanic region correlates again at a four month lag with all but zone 3, as does the CEI region at a three month lag. The EEI region correlates at a three month lag with all except zone 4 as does the SEI regions which also correlates at a three month lag. In this month the tele-connections move away from the coastal key–box areas back to the northern Indian Ocean. It shows the association between a lower latent heat flux anomalies and an increase in rainfall exists. The regions which correlated at a three month lag, that is the December latent heat flux and March rainfall seem to dominate the picture. This suggests that if there is lower than average latent heat flux in these regions there will be higher than average rainfall in Southern Africa. This could be due to the fact that the moisture is not lost further north on the African continent, but rather the rains precipitate further south.

6.3 Discussion of results

As stated in section 1.1: "The main objective of this study was to determine if there is a useful link between oceanic latent heat flux and South Africa's summer monthly rainfall patterns. Useful in the sense that it adds to our knowledge and in the sense that with this we can effectively predict to some degree the rainfall variability." As rainfall is one of the key elements in climate variability some degree of prediction is of benefit. As stated earlier, the main purpose of Esbensen and Reynolds (1981) paper was to provide a basis for determining to what extent the classical method of calculating fluxes of sensible and latent heat from monthly averaged meteorological variables can be used for studies on the order of interannual and decadal climatic variability. They suggest that the classical method of calculating oceanic heat flux was successful in monitoring interannual variability.

On examining the results of this study the following facts where observed:

- The rainfall regions can be effectively combined to form an all-area index.
- It is not possible to average early (October to December) and late (January to March) summer months as different factors produce rainfall in each of the months.
- There appear to be three major "mechanisms" at work over the six month summer period.

We will discuss each of these factors in more detail below

Firstly, in examining the results of this study it is clear that the separate rainfall zones can be effectively combined to form an all-area index. Although some of the particular rainfall zones (one to four) do not always have the same correlation as the all-area indexes (zones seven and eight), the majority of the rainfall patterns over the area correlated and to simplify the prediction of rainfall it is sufficient to work with an all-area index. The relationship between the various summer rainfall zones and the two all-area indexes is shown in tables 6.1 to table 6.6

Secondly, it is not possible to have an early and late summer rainfall season by averaging the three early and three late months. The results lead one to the conclusion that there are different mechanisms at work in the different months, and even in adjacent months. This would preclude one from then forming a early or later summer rainfall index.

Thirdly, there appear to be three major "mechanisms" at work in the summer rainfall zones. If we look at the

oceanic latent heat flux regions and the correlation with the rainfall of zone eight, which is a proxy of all the summer rainfall zones considered, the following is clear:

In the month of October, there is a significant negative correlation with the oceanic latent heat flux anomalies in the EEI region at both a one and three month lag, with all the three month lag correlations at greater than the 95 % confidence level. There are also positive correlations with the ARR region at a shorter lag of one month. The three month correlation is between the October rainfall and the proceeding July's oceanic latent heat flux. Oceanic latent heat flux in this area increases from its average of 80 $W.m^{-2}$ in April to between 120–160 $W.m^{-2}$ in July (Godffey et al. 1995). Pathack (1993) did not consider October rainfall variations as this month was the driest of the six months considered in his study.

In November the correlation pattern changes with the only significant correlation being with ASA region. The significance of the correlation for the ASA region and zone 8 rainfall is over 98%. This could be linked to the winter Monsoon of the Northern hemisphere, as the month of November is regarded as one of the transitional months (Tomczak and Godfrey 1994) from a summer Southwest Monsoon to a winter Northeast Monsoon. The ASA region is oceanographically dominated by the relatively cold Somali Current, which is established in response to the wind reversal along the African coast (Tomczak and Godfrey 1994). Godffey et al. (1995) state that unlike most of the northern Indian Ocean, which has a nearly uniform latent heat flux of 80 $W.m^{-2}$ in April and an increase to between 120–160 $W.m^{-2}$ in July, the Arabian Sea remains relatively cloud free so solar radiation input remains constant and the latent heat lost remains near 80 $W.m^{-2}$. A change in the amount of incoming solar radiation can upset the total heat flux balance resulting in changes in the oceanic heat flux. These effects are then felt in a change in the rainfall patterns. This is also an important month as it is the start of the South African agricultural growing season. Pathack, Jury, Shillington, and Courtney (1993) state that the November precipitation was more frequent from cold systems which might benefit from surface heat inputs in the south-west or west of the southern African subcontinent through a re-orientation of standing subtropical wave patterns.

In December, the dominance of the ASA regions continues with negative lag correlations at two and three months. At a two months lag this is with the October ASA oceanic latent heat flux, which was discussed before. The EEI region once again appears significant but at a positive four month lag. Pathack (1993) noted an association with the ASA region. In fact it he noted that December to March rainfall across the summer rainfall region of South Africa were more frequently produced from warm systems where convergence and east–west Walker cell–type circulations were

most important.

The January results show a complete change in the pattern with the only consistent correlations being with the oceanic regions adjacent to Southern Africa, the ARR and the BCR regions. Both these regions correlate negatively and simultaneously with the rainfall.

In February a similar pattern exists with the regions nearest the coast correlating with the rainfall zone. However, these correlations are lagged, two months in the case of the ARR region and five months in the case of the ACR region. Both these sets of correlations are significant at greater than 90 %. Jury (1995) in his review paper, states that there is a high spatial correlation of 0.95 between SST in the surrounding area and February rainfall. This confirms that SST may directly affect the convective potential on sub-tropical weather systems. The higher correlation in February is probably due to the more gradual eastward movement of associated air-sea interaction.

March once again shows a change in the predominant patterns that held for January and February. In this month the WEI, CEI, EEI and SEI regions all correlated significantly with the rainfall. With the exception of the WEI region, which correlates at a zero lag and four month lag, all the regions show a three month lag in correlation with the rainfall. All these correlations, including the WEI region, are positive, unlike the negative correlations of the EEI region in the previous October. It has been suggested that the SST of the CEI region controls the major mode of inter-annual climatic variability over southern Africa (Jury 1995). Pathack (1993) found that the Indian Ocean is "upstream" at this time owing to the seasonal oscillation of mid-tropospheric and sub-tropical zonal winds. He also found a negative relationship between SST and the SEI region. It was suggested that the physical reason for this is that with an increase in SST, there was a tendency for intense tropical cyclones to be more frequent during the austral summer, and this had the effect of depriving the southern African subcontinent of moisture flux.

These results are summarized in the table 6.7.

Month	Region(s)				
October	-EEI-1	-EEI-3	ARR-1		
	-0.29	-.036	0.30		
November	-ASA-1				
	-0.41				
December	-ASA-2	-ASA-3	EEI-4		
	-0.38	-0.38	0.35		
January	-ARR-0	-BCR-0			
	-0.37	-0.42			
February	-ARR-2	-ACR-5			
	-0.37	-0.50			
March	WEI-0	WEI-4	CEI-3	EEI-3	SEI-3
	0.36	0.41	0.38	0.38	0.34

Table 6.7: Summary of the major results: Rainfall for Zone 8 vs. Oceanic Latent Heat Flux in the Key Boxes (90 % significance level is 0.28 and the 95 % significance level is 0.33)

6.3.1 The problems encountered

The problems encountered in this study fall into two general areas. These are (a) specifically data related and (b) methods used in the computation of the data. We shall examine each of these in turn:

Data resolution problems

The data that was used in this study were the COADS Monthly Summary Trimmed Group data set. Problems that were, encountered in general with that data set were outlined in section 4.2.2.

However, when we consider using the data to calculate monthly heat flux values, other problems arise. Firstly

the temporal resolution is such that we only have monthly data for the parameters we need for our calculations. In the case of latent heat flux, we only had the monthly average values of SST, specific humidity, vector winds and sea level pressure. From these the other variables that were needed were derived. This means that the equation 2.11 was used to calculate the oceanic latent heat flux. This formula has been shown to give a 10% relative error over equation 2.9. To form the various oceanic latent heat flux regions, spatial averaging was used, this has the further effect of decreasing the random errors. The relative error of 10 % is dismissed in this study as we are not using the actual values themselves, but rather the anomalies of these values

Secondly the spatial resolution is two degrees. This posses the problem that the heat flux is calculated over a relatively large area. This kind of problem can only be reduced by calculating the heat flux using equation 2.9 where the values of Q_s and Q_a are calculated at each data point. As we consider only large scale disturbances in the latent heat flux field to be important this aspect too has been disregarded in this study. Ideally one should have both higher temporal and spatial resolution of data so that a more accurate oceanic heat flux field can be calculated. Unfortunately, such data on a long time scale does not exist.

Methods used for computing the heat flux data

Computationally, problems that occurred are a direct result of the nature of data used and the difficulty of accurately calculating oceanic heat flux over a large area. The only formula that could be used to calculate the oceanic heat flux were those formulae that are known as the bulk aerodynamic formulae. The derivation of the formula for latent and sensible heat flux is shown in Chapter 4.

By far the most wide reaching problem in calculation of heat flux is the so called "transfer co-efficents" and which one(s) to use. The calculation of suitable co-efficents are notorious and have presented numerous problems to researchers. Some of these problems and solutions have been covered in section 2.2. One needs to accept that the Bulk Aerodynamic Method of calculating oceanic heat flux has inaccuracies, which according to Blanc (1987), were between 35–200%.

However, since this study was involved in using the relative fluctuations of the oceanic heat flux fields, that is the oceanic heat flux fields are normalized, it is assumed that these absolute errors present less of a problem with a relative study of the oceanic heat flux anomalies. In this study the use of area averages of latent heat flux also reduced

random errors that occur in the data. This was seen when looking at point to field correlations versus field to field correlations. In the first case the results show a random scatter with very little coherency as illustrated in figure 5.1. Much more useful results were obtained using a field to field correlation and it was these results that were used in this dissertation.

6.4 Conclusions and Future Studies

In order to keep these conclusions focused, let us examine the results in light of the initial objectives outlined in section 1.1. Firstly, we needed to ascertain if there was a useful link between oceanic latent heat flux and southern African summer rainfall. This study has shown that various oceanographic areas in the surrounding oceans correlate at different lags with rainfall. These correlations can be useful as precursors in predicting wetter or dryer rainfall events. Secondly, we asked the question as to whether this study adds to our knowledge in the sense that with this we can effectively predict to some degree the rainfall variability. This too has been shown in the various correlations of the oceanic latent heat flux and rainfall for the different summer rainfall months. Areas identified as important as precursors for summer rainfall prediction are similar to those areas other researches have identified in studies using OLR, SST and upper level winds (Jury 1995). This study adds weight to the already existing knowledge of these precursors of rainfall predictability.

This study has shown that oceanic latent heat flux in the key oceanic boxes identified can be used in the prediction of rainfall trends in the summer rainfall regions of southern Africa. With the lag correlations being with zones in the Indian Ocean, they should be seen as precursors of summer rainfall patterns rather than as mechanisms causing summer rainfall patterns.

This study did not show the relationship between cause and effect in the thermodynamic process at work in ocean–atmosphere coupling. A statistical relationship has been explored in this study as a basis for future work. This will most probably be carried out using high resolution measurements of the total heat budget and use of numerical models.

In one such study done by White (1995) an intercomparison of four GCM's with respect to precipitation, surface fluxes and top-of-the atmosphere OLR were compared. This study showed that the models compared well and realistically depicted the large interannual variations in precipitation. Although the models agree well on oceanic surface

fluxes and agree on the pattern of surface fluxes over land, the magnitudes do not agree well. A major source of uncertainty is the cloudiness. If these problems could be better parameterized the usefulness of GCM's in predicting seasonal changes could well prove useful. However, with any coupled ocean–atmosphere model we must add that a model only reproduces a picture of the real world, only in the framework defined by the limitation of our knowledge about the processes which occur in it (Kagan 1995).

In order to do long-range forecasting it is impractical to get accurate readings of atmospheric and oceanic variables over the entire ocean. However, one needs to develop a system where by the few accurate readings we have are effectively integrated into a good GCM. This will lead to the GCM's producing better results along with a feed back to the community as to the effectiveness of the models flux calculations.

Glossary

This is a glossary of terms used.

AVHRR	Advanced Very High Resolution Radar
BMRC	Bureau of Meteorology Research Centre
CCWR	Computing Centre for Water Research
CIRES	Cooperative Institute for Research in Environmental Sciences
CMR	Compressed Marine Reports
COADS	Comprehensive Ocean–Atmosphere Data Set
CPU	Central Processing Unit
ECMWF	European Center for Medium Range Weather Forecasts
ENSO	El Niño Southern Oscillation
EOF	Empirical Orthoganal Functions
GARP	Global Atmospheric Research Programme
GLA	Goddard Laboratory for Atmospheres
HEXOS	Heat Exchange of the Sea
HSST	Historical Sea-Surface Temperature
ITCZ	Inter Tropical Convergence Zone
MSTG	Monthly Summary Trimmed Group
NCAR	National Centre for Atmospheric Research
NCDC	National Climatic Data Center
NMC	U.S. National Meteorological Centre

NOAA National Oceanic and Atmospheric Administration

OLR Outgoing Longwave Radiation

PCA Principle Component Analysis

REOF Rotated Empirical Orthoganal Functions

RMS Root Mean Square

SLP Sea Level Pressure

SO Southern Oscillation

SOI Southern Oscillation Index

SST Sea Surface Temperature

TDF Tape Data Format

TIROS-N Television infared observation satellite

WMO World Meteorological Organisation

Appendix A

Statistical Methods used in this study

In the appendix we look a the methods that were applied to the data to normalise it as well as the correlation methods used for the computation of the correlation coefficient.

A.1 Normalisation

Normalisation is a very useful process when it is required to produce indices from various stations with differing characteristics. One such example is rainfall data in regions that receive their rainfall from convective systems. These systems are "noisy", in the sense that a few isolated perturbations produce transient excess rainfall at a few stations, while stations in the nearby area remain relatively dry. In situations, arithmetic averaging of data will not provide a good "average" value. One method of combining data from various locations within a given region is through normalisation (Kraus, 1977). This method provides a useful index (e.g standardised rainfall index) for a particular area. These indices calculated as shown in equation A.1 have a zero mean and a unit variance.

$$Z_i = \frac{X_i - \mu}{\sigma} \sim N(0,1) \tag{A.1}$$

where X_i = the variable to be normalised

μ = the mean (of the distribution) of the variable

σ = the standard deviation (of the distribution) of the variable

Areal indices are formed by averaging over all the individual station indices within the area concerned.

A.2 Correlation And Significance Tests

The statistical technique of correlation analyses has been used extensively in climatology as a tool for assessing the strength of different relationships among variables (Pathack 1993). The major problem is that this technique may lead to false conclusions as these tests have no built in ability to distinguish between cause and effect.

The strength of the correlation coefficient (r) is a value that varies between -1 and 1. If r is positive then both the dependent and independent variables increase or decrease together. If r is negative then the dependent and independent variable move in opposite directions. If the value is close to $\mid 1 \mid$ then the correlation is perfect, but if r is close to 0 the correlation is poor.

To test how "good" the correlation coefficient is, the square of the correlation coefficient (r^2) is calculated. This value shows the percentage of the total variation of the dependent variable that can be explained by the independent variable.

The more commonly used Pearson correlation coefficient can be calculated using the formula give in equation A.2.

$$r = \frac{\sum_{i=1}^{N}(x_i - \overline{x})(y_i - \overline{y})}{\sqrt{\sum_{i=1}^{N}(x_i - \overline{x})^2}\sqrt{\sum_{i=1}^{N}(y_i - \overline{y})^2}} \tag{A.2}$$

The test for the significance of the Pearson correlation coefficient is given in equation A.3. This test is to see if r, which is an estimate of the true correlation coefficient which measures the degree of interrelationship between the dependent and independent variables. Since r is a sample estimate, we must test its statistical reliability by conducting the appropriate test of significance. This is done by applying the Students t test to the value. This test does, however, rely on a degree of normality of the frequency distributions of the data sets involved.

$$t = r\sqrt{\frac{N-2}{1-r^2}} \tag{A.3}$$

A second method of calculating a correlation coefficient is to use the Spearman rank correlation coefficient r_s. This is calculated using equation A.4. Here instead of using the actual values, the two given series are first ranked in order of size. These ranks are then correlated. This is a non parametric test.

$$r_s = \frac{\sum_{i=1}^{N}(R_i - \overline{R})(S_i - \overline{S})}{\sqrt{\sum_{i=1}^{N}(R_i - \overline{R})^2}\sqrt{\sum_i (S_{i=1}^{N} - \overline{S})^2}} \tag{A.4}$$

It sometimes turns out that this is equal to another conventional measure of non parametric correlation known as the sum square difference of ranks, defined here in equation A.5

$$D = \sum_{i=1}^{N}(R_i - S_i)^2 \tag{A.5}$$

When there are no ties in the data then the exact relationship between D and r_s is give in equation A.6.

$$r_s = 1 - \frac{6D}{N^3 - N} \tag{A.6}$$

When there are ties, then things are more complicated. To solve for this we let f_k be the number of ties in the k^{th} group of ties among the R_i's and then let g_k be the number of ties in the m^{th} group of ties among the S_i's. It turns out that

$$r_s = \frac{1 - \frac{6D}{N^3-N}\left[D + \frac{1}{2}\sum_k (f_k^3 - f_k) + \frac{1}{2}\sum_m (g_m^3 - g_m)\right]}{\left[1 - \frac{\sum_k (f_k^3 - f_k)}{N^3-N}\right]\left[1 - \frac{\sum_m (g_m^3 - g_m)}{N^3-N}\right]} \tag{A.7}$$

holds exactly. (Note if all the f_k's and all the g_k's are equal to one, then equation A.7 reduces to the previous equation A.6) .

The test for the significance of the Spearman rank correlation coefficient is given in equation A.8. This is always a good test because this coefficient does not rely on the data itself, but rather on its ranking.

$$t = r_s\sqrt{\frac{N-2}{1-r_s^2}} \tag{A.8}$$

In this study both the Pearson product moment correlation coefficient and the Spearman rank correlation coefficient were used. In each case the relevant Student–t test was used to show the significance of the test.

Bibliography

Atlas, R. (1987). The role of oceanic fluxes and initial data in the numerical prediction of an intense coastal storm. *Dynamics of Atmospheres and Oceans 10*, 359–388.

Berlage, H. P. (1957). Fluctuations of the general atmospheric circulation of more than one year, their nature and prognostic value. *Medelelingen en Verhandelingen. Koninklijk Nederlands Meteorologisch Instituut 69*, 152pp.

Berlage, H. P. (1966). The Southern Oscillation and world weather. *Medelelingen en Verhandelingen. Koninklijk Nederlands Meteorologisch Instituut 88*, 152pp.

Blanc, T. V. (1985, June). Variation of bulk-derived surface flux, stability, and roughness results due to the use of different transfer coefficient schemes. *Journal of Physical Oceanography 15*, 650–669.

Blanc, T. V. (1987, April). Accuracy of bulk-method-determined flux stability, and sea surface roughness. *Journal of Geophysical Research 92*(C4), 3857–3876.

Bolton, D. (1980, July). The computation of equivalent potential temperature. *Monthly Weather Review 108*, 1046–1053.

Bunker, A. F. (1976, September). Computations of surface energy flux and annual air-sea interaction cycles of the North Atlantic Ocean. *Monthly Weather Review 104*, 1122–1139.

Cane, M. (1986). El niño. *Annual review of Earth and Planetary Science*, 43–70.

Cayan, D. R. (1992a, August). Latent and sensible heat flux anomalies over the northern oceans: Driving the sea surface temperature. *Journal of Physical Oceanography 22*, 859–881.

Cayan, D. R. (1992b, April). Latent and sensible heat flux anomalies over the northern oceans: The connection to monthly atmospheric circulation. *Journal of Climate 5*(4), 354–369.

Cayan, D. R. (1992c). Variability of latent and sensible heat fluxes estimated using bulk formulae. *Atmosphere-Ocean 30*(1), 1–42.

Crewell, S., E. Ruprecht, and C. Simmer (1991, December). Latent heat flux over the North Atlantic Ocean—A case study. *Journal of Applied Meteorology 30*, 1627–1635.

Esbensen, S. K. and R. W. Reynolds (1981, April). Estimating monthly averaged air-sea transfers of heat and momentum using the bulk aerodynamic method. *Journal of Physical Oceanography 11*, 457–465.

Foster, R. C. and R. A. Brown (1994). On large-scale PBL modelling: Surface wind and latent heat flux comparisons. *The Global Atmosphere and Ocean System 2*, 199–219.

Friehe, C. A. and K. F. Schmitt (1976, November). Parameterization of air-sea interface fluxes of sensible heat and moisture by the bulk aerodynamic formulas. *Journal of Physical Oceanography 6*, 801–809.

Godffey, J. S., A. Alexiou, A. G. Ilanhude, D. M. Legler, M. E. Luther, J. J. P. McCreary, G. A. Meyers, K. Mizumo, R. R. Rao, S. R. Meyers, J. H. Toole, and S. Wacongne (1995, February). The role of the Idian Ocean in the Global Climate System: Recommendations regarding the Global Ocean Observing System. Technical report, Ocean Observing System Development Panel, Texas A&M University, College Station, TX, U.S.A.

Gordon, H. R. and B. G. Hunt (1991). Droughts, floods, and sea-surface temperature anomalies: A modelling approach. *International Journal of Climatology 11*, 347–365.

Grachev, A. A. and G. N. Pannin (1984). Parameterization of the sensible and latent heat flux above the water surface in calm weather under natural conditions. *Izvestiya, Atmospheric and Oceanoc Physics 20*(5), 371–376.

Gueremy, J. F. (1990). Heat and moisture fluxes on the time scale of 20 to 60 days over the Indian Monsoon area. *Meteorology and Atmospheric Physics 44*, 219–250.

Harrison, M. S. J. (1983). Rain day frequency and mean daily rainfall intensity as determinants of total rainfall over the eastern Orange Free State. *Journal of Climatology 3*, 35.

Harrison, M. S. J. (1984). A generalized classification of South African summer rain-bearing synoptic systems. *Journal of Climatology 4*, 547–560.

Harrison, M. S. J. (1986). *A Synoptic Climatology of South African Rainfall Variations*. Ph. D. thesis, University of the Witwatersrand.

Hastenrath, S. and P. J. Lamb (1980, May). On the heat budget of hydrosphere and atmosphere in the Indian Ocean. *Journal of Physical Oceanography 10*, 694–708.

Hildebrandsson, H. H. (1897). Quelques recherches sur les entres d'action de l'atmosphere. *Konglica Svenska Vetenskapskademiens Handlingar 29*, 33pp.

Hsiung, J. (1986, September). Mean surface fluxes over the global ocean. *Journal of Geophysical Research 91*(C9), 10585–10606.

Hsu, S. A. (1988). *Coastal Meteorology*. Academic Press, Inc.

Jury, M. and N. Walker (1988, January). Marine boundary layer modification across the edge of the Agulhas Current. *Journal of Geophysical Research 93*(C1), 647–654.

Jury, M. R. (1995, June). A review of research on ocean - atmosphere interactions and South African climate variability. *South African Journal of Science 91*, 289–294.

Kagan, B. A. (1995). *Ocean–Atmosphere Interaction and Climate Modelling*. Cambridge University Press. Translated by Mikhail Hazin.

Lambert, S. J. and G. J. Boer (1989). Atmosphere-ocean heat fluxes and stresses in general circulation models. *Atmosphere-Ocean 27*(4), 692–715.

Large, W. G. and S. Pond (1982, May). Sensible and latent heat flux measurements over the ocean. *Journal of Physical Oceanography 12*, 464–482.

Leslie, L. M., G. J. Holland, and A. H. Lynch (1987, December). Australian east-coast cyclones: Part II: Numerical modeling study. *Monthly Weather Review 115*, 3037–3053.

Lindesay, J. A. (1988a). South African rainfall, the Southern Oscillation and a southern hemisphere semi-annual cycle. *Journal of Climatology 8*, 17–30.

Lindesay, J. A. (1988b). *The Southern Oscillation and Atmospheric Circulation Changes over Southern Africa*. Ph. D. thesis, University of the Witwatersrand.

Liu, W. T. (1986, August). Statistical relation between monthly mean precipitable water and surface-level humidity of global oceans. *Monthly Weather Review 114*(8), 1591–1602.

Lockyer, N. and W. J. S. Lockyer (1902). On the similarity of the short-period pressure variation over large areas. *Proceedings of the Royal Society of London 73*, 459–470.

Mey, R. D., N. D. Walker, and M. R. Jury (1990, September). Surface heat fluxes and marine boundary layer modification in the Agulhas Retroflection region. *Journal of Geophysical Research 95*(C9), 15997–16015.

Miller, M. J., A. C. M. Beljaars, and T. N. Palmer (1992, May). The sensitivity of the ECMWF model to the parameterization of evaporation from tropical oceans. *Journal of Climate 5*, 418–434.

Namias, J. (1973). Thermal communication between the sea surface and the lower troposphere. *Journal of Physical Oceanography 3*, 373–378.

Namias, J. and D. R. Cayan (1981, November). Large-scale air-sea interactions and short period climate fluctuations. *Science 214*(4523), 869–876.

Palmer, T. N., Č. Branković, F. Molteni, and S. Tibaldi (1990). Extended-range predictions with ECMWF models: Interannual variability in operational model integrations. *Quarterly Journal of the Royal Meteorological Society 116*, 799–834.

Pathack, B. M. R. (1993, August). *Modulation of South African Summer Rainfall by Global Climatic Processes.* Ph. D. thesis, University of Cape Town.

Pathack, B. M. R., M. R. Jury, F. A. Shillington, and S. Courtney (1993, May). South African summer rainfall variability and its association with the surrounding marine environment. Technical report, Water Research Commission.

Philander, S. G. H. (1983). El niño Southern Oscillation phenomena. *Nature 302*, 295–301.

Reed, R. J., A. J. Simmons, M. D. Albright, and P. Undèn (1988, September). The role of latent heat release in explosive cyclogenesis: Three examples based on ECMWF operational forecasts. *Weather and Forecasting 3*, 217–229.

Ruprecht, E. and C. Simmer (1991). Fluxes of latent heat over the ocean: climatological studies and application of satellite observations. *Dynamics of Atmospheres and Oceans 16*, 111–121.

Simonot, J. Y. and H. L. Treut (1987). Surface heat fluxes from a numerical weather prediction system. *Climate Dynamics 2*, 11–28.

Slutz, R. J., S. J. Lubker, J. D. Hiscox, S. D. Woodruff, R. L. Jenne, D. H. Joseph, P. M. Steurer, and J. D. Elms (1985). Comprehensive Ocean-Atmosphere Data Set; release 1. Technical report, NOAA Environmental Research Laboratories, Climate Research Program.

Smith, S. D. (1980). Wind stress and heat flux over the ocean in gale force winds. *Journal of Physical Oceanography 10*, 709–726.

Smith, S. D. (1989). Water vapour flux at the sea surface (review paper). *Boundary layer Meteorology 47*, 277–293.

Tomczak, M. and J. S. Godfrey (1994). *Regional Oceanography: An Introduction*, Chapter 11. Pergamon.

Tyson, P. D. (1984). The atmospheric modulation of extended wet and dry spells over South Africa, 1958–1978. *Journal of Climatology 4*, 621–635.

Tyson, P. D. (1986). *Climatic Change and Variability in Southern Africa.* Oxford University Press, Cape Town.

Walker, G. T. (1923). Correlation in seasonal variations of weather, VIII. a preliminary study of world weather (world weather I). *Memoirs of the Indian Meteorological Department 24*(4), 75–131.

Walker, G. T. (1924). Correlation in seasonal variations of weather, IX. a further study of world weather (world weather II). *Memoirs of the Indian Meteorological Department 24*(9), 275–332.

Walker, N. D. (1989, April). *Sea Surface Temperature-Rainfall Relationships and Associated Ocean-Atmosphere Coupling Mechanisms in the Southern African Regions.* Ph. D. thesis, University of Cape Town.

Walker, N. D. (1990, March). Links between South African summer rainfall and temperature variability of the Agulhas and Benguela current systems. *Journal of Geophysical Research 95*(C3), 3297–3319.

Weare, B. C. and T. Strub (1981, April). The significance of sampling biases on calculated monthly mean oceanic surface heat fluxes. *Tellus 33*(2), 211–224.

White, G. H. (1995, November). An intercomparison of precipitation and surface fluxes from operational nwp analysis/forecast systems. Technical Report WMO/TD-No. 723, Environmental Modelling Center, National Centers for Environmental Prediction, Washington, DC, USA.

Woodruff, S. D., R. J. Slutz, R. L. Jenne, and P. M. Steurer (1987, October). A Comprehensive Ocean-Atmosphere Dat Set. *Bulletin of the American Meteorological Society 68*(10), 1239–1250.

Wu, J. (1992, March). Variation of the heat and transfer coefficients with environmental parameters. *Journal of Physical Oceanography 22*, 293–300.

Yarnal, B. (1985). Extratropical teleconnections with El Niño/Southern Oscillation (ENSO) event. *Progress in Physical Geography 9*, 315–352.

Yarnal, B. and G. Kiladis (1985). Tropical teleconnections associated with El Niño/Southern Oscillation (ENSO) event. *Progress in Physical Geography 9*, 524–558.